Me**A**surement of the F_2^n/F_2^p and d/u **RA**tios in Deep Inelastic Electron Scattering off the **T**ritium and **H**elium Mirr**O**r **N**uclei.

Jefferson Lab PAC27 Proposal

December 2004

The JLab **MARATHON** Collaboration

K. A. Aniol, D. J. Margaziotis, M. B. Epstein
California State University, Los Angeles, California, USA

G. Fanourakis
Demokritos National Center for Scientific Research, Athens, Greece

J. Annand, D. Ireland, R. Kaiser, G. Rosner
University of Glasgow, Scotland, UK

M. E. Christy, C. E. Keppel, V. Tvaskis
Hampton University, Hampton, Virginia, USA

E. Cisbani, F. Cussano, S. Frullani, F. Garibaldi, M. Iodice, L. Lagamba
R. De Leo, E. Pace, G. Salmè, G. M. Urciuoli
Istituto Nazionale di Fisica Nucleare, Rome and Bari, Italy

J. Gomez, C. W. de Jager, W. Melnitchouk, S. K. Nanda
Jefferson Lab, Newport News, Virginia, USA

B. D. Anderson, A. T. Katramatou, E. Khrosinkova, D. M. Manley,
S. Margetis, G. G. Petratos, W.-M. Zhang
Kent State University, Kent, Ohio, USA

J. R. Calarco
University of New Hampshire, Durham, New Hampshire, USA

C. Ciofi degli Atti, S. Scopetta
University of Perugia, Perugia, Italy

R. Gilman, C. Glashausser, R. D. Ransome, X. Ziang
Rutgers, The State University of New Jersey, New Brunswick, New Jersey, USA

S. Liuti, O. Rondon
University of Virginia, Charlottesville, Virginia, USA

Spokesperson: G. G. Petratos (gpetrato@kent.edu)

Co-spokespersons: J. Gomez and R. D. Ransome

ABSTRACT

We propose to measure the ratio of the neutron to proton inelastic structure functions, F_2^n/F_2^p, and the ratio of the down to up quark distributions in the nucleon, d/u, at medium and large Bjorken x, by performing deep inelastic electron scattering off ^{3}He and ^{3}H with the 6 GeV upgraded beam of Jefferson Lab. The experiment will use room-temperature gas targets pressurized to 11 atm, and either the Hall A High Resolution Spectrometer system or the Hall C High Momentum Spectrometer system for the detection of scattered electrons. The required beam time is 35 days at a canonical beam current of 100μA. The F_2^n/F_2^p ratio will be extracted from the inelastic cross section ratio of the two nuclei by exploiting their mirror symmetry with a minimal theoretical correction. The F_2^n/F_2^p ratio is expected to be almost free of nuclear effects, which introduce a significant uncertainty in its extraction from deep inelastic scattering off the proton and deuteron. The results are expected to test perturbative and non-perturbative mechanisms of spin-flavor symmetry breaking in the nucleon, and constrain the structure function parametrizations needed for the interpretation of high energy hadron collider data. The experiment will also measure the absolute value of the inelastic cross sections for the two nuclei and determine the magnitude and x-dependence of their nuclear EMC effect. The precision of the expected cross section data will offer a unique opportunity to test competing parametrizations of the EMC effect and it will provide critical experimental input for the establishment of a unique canonical model for the explanation of the dynamical origin of the effect. A by-product of this experiment will be a substantial improvement of the quality of the existing data on the tritium elastic form factors, which will constrain theoretical calculations for the three-body systems.

1 Introduction

Measurements of the proton and deuteron structure functions have been of fundamental importance in establishing the internal quark structure of the nucleon [1, 2, 3]. The first evidence for the presence of point-like constituents (partons) in the nucleon came from the observation that the ratio of inelastic to Mott electron-proton cross sections, measured in the pioneering SLAC experiments, exhibited only small variation with momentum transfer [4]. The subsequent detailed analysis of the SLAC data [5] revealed the predicted "scaling pattern" [6] in the nucleon structure functions, consistent with scattering from partons carrying the quantum numbers of the Gell-Mann/Zweig quarks. Further experimental studies of muon-nucleon and neutrino-nucleon inelastic scattering experiments at CERN and Fermilab established beyond any doubt the quark-parton model (QPM) of the nucleon [7], and provided substantial supporting evidence for the emerging theory of quantum chromodynamics (QCD) [8].

The cross section for inelastic electron-nucleon scattering is given in terms of the structure functions $F_1(\nu, Q^2)$ and $F_2(\nu, Q^2)$ of the nucleon by:

$$\sigma \equiv \frac{d^2\sigma}{d\Omega dE'}(E, E', \theta) = \frac{4\alpha^2(E')^2}{Q^4}\cos^2(\frac{\theta}{2})\left[\frac{F_2(\nu, Q^2)}{\nu} + \frac{2F_1(\nu, Q^2)}{M}\tan^2(\frac{\theta}{2})\right] , \tag{1}$$

where α is the fine-structure constant, E is the incident electron energy, E' and θ are the scattered electron energy and angle, $\nu = E - E'$ is the energy transfer, $Q^2 = 4EE'\sin^2(\theta/2)$ is minus the four-momentum transfer squared, and M is the nucleon mass.

The basic idea of the quark-parton model [6, 9] is to represent inelastic electron-nucleon scattering as quasi-free scattering from the partons/quarks in the nucleon, when viewed in a frame where the nucleon has infinite momentum (the center-of-mass frame is a very good approximation to such a frame). The fractional momentum of the nucleon carried by the struck quark is given by the Bjorken scaling variable, $x = Q^2/2M\nu$. In the limit where $\nu \to \infty$, $Q^2 \to \infty$ with x fixed, the nucleon structure functions become:

$$F_1 = \frac{1}{2}\sum_i e_i^2 q_i(x) , \qquad F_2 = x\sum_i e_i^2 q_i(x) . \tag{2}$$

Here, e_i is the fractional charge of quark type i, $q_i(x)dx$ is the probability that a quark of type i carries momentum in the range between x and $x+dx$, and the sum runs over all quark types.

Since the charges of the u, d and s quarks are $2/3$, $-1/3$ and $-1/3$, respectively, the $F_2(x)$ structure function for the proton is given by:

$$F_2^p(x) = x\left[\left(\frac{2}{3}\right)^2(u+\bar{u}) + \left(-\frac{1}{3}\right)^2\left(d+\bar{d}\right) + \left(-\frac{1}{3}\right)^2(s+\bar{s})\right] . \tag{3}$$

The parton distribution functions in the neutron are related to those in the proton by isospin symmetry. Since the up/down quarks and proton/neutron both form isospin doublets, one has: $u^p(x) = d^n(x) \equiv u(x)$, $d^p(x) = u^n(x) \equiv d(x)$, $s^p(x) = s^n(x) \equiv s(x)$ (with analogous relations for the antiquarks), and:

$$F_2^n(x) = x\left[\left(-\frac{1}{3}\right)^2(u+\bar{u}) + \left(\frac{2}{3}\right)^2\left(d+\bar{d}\right) + \left(-\frac{1}{3}\right)^2(s+\bar{s})\right] . \tag{4}$$

Equations 3 and 4 result in the structure function ratio:

$$\frac{F_2^n}{F_2^p} = \frac{[(u+\bar{u}) + (s+\bar{s})] + 4(d+\bar{d})}{4(u+\bar{u}) + [(d+\bar{d}) + (s+\bar{s})]} . \tag{5}$$

Since all the quark distribution functions must be positive for all x, the above expression is bounded for all x by:

$$\frac{1}{4} \leq \frac{F_2^n}{F_2^p} \leq 4 , \tag{6}$$

which is known as the Nachtmann inequality [10]. If one neglects the strange quarks and antiquarks, Equation 5 yields the well known simple relationship:

$$\frac{F_2^n}{F_2^p} = \frac{[(u+\bar{u})] + 4(d+\bar{d})}{4(u+\bar{u}) + [(d+\bar{d})]} = \frac{1+4(D/U)}{4+(D/U)} , \tag{7}$$

where $U = u + \bar{u}$ and $D = d + \bar{d}$. For the remainder of this proposal the notation D/U will be replaced, as it is customary, simply by d/u, with d and u denoting quark plus antiquark distributions. Figure 1 shows all the SLAC data from the pioneering SLAC/MIT Collaboration experiments on the F_2^n/F_2^p ratio versus x [11]. The ratio has been extracted from deep inelastic scattering (DIS) (large Q^2 and ν) measurements off the proton and deuteron, using a smearing model to account for the Fermi-motion of the nucleons in the deuteron [12]. The ratio data are within the bounds of the Nachtmann inequality. For large x, the ratio is about $1/4$ which can only be reached if $d = \bar{d} = s = \bar{s} = 0$. This suggests a picture in which the high momentum partons in the proton (neutron) are mainly up (down) quarks. For small x, the ratio is close to 1, suggesting little influence of valence quarks and dominance of the quark-antiquark "sea".

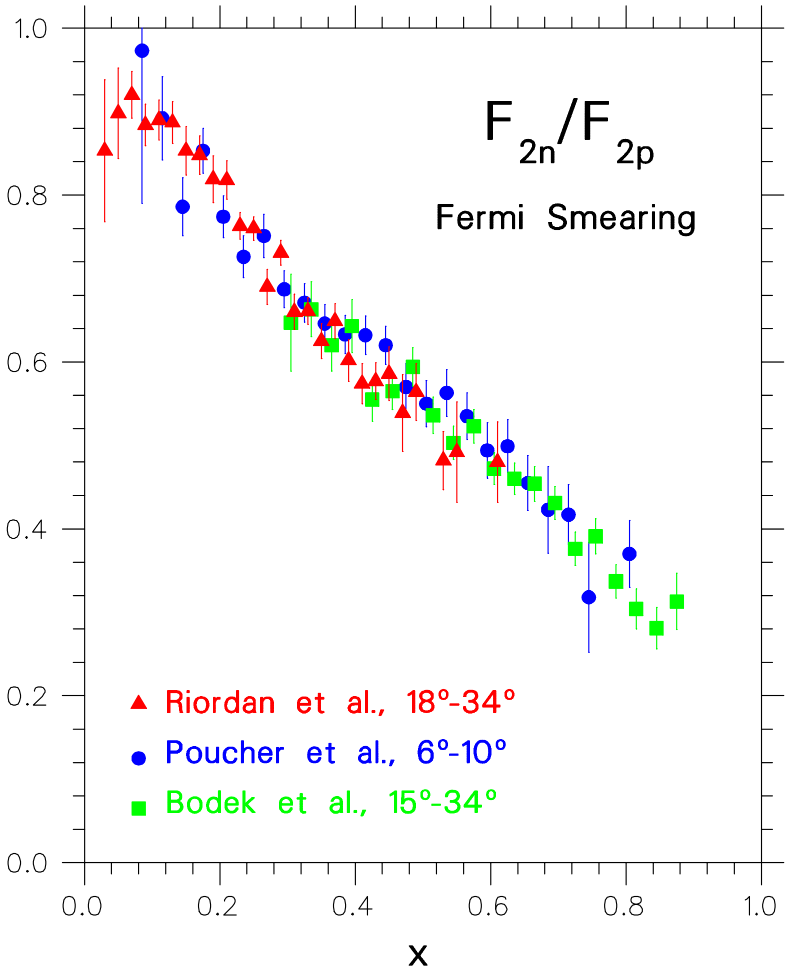

Figure 1: SLAC data on the nucleon F_2^n/F_2^p ratio extracted from proton and deuteron DIS measurements [11] with a Fermi-smearing model [12].

Early SLAC experimental data in a limited x kinematical range ($0.1 \leq x \leq 0.3$) [13] reinforced an original naive view that the quark distributions functions $q_i(x)$ should not change in the nuclear medium, at least for small and medium values of x. Measurements by the European Muon Collaboration (EMC) [14] over a large-x range at CERN invalidated this view by observing a large x dependence for the ratio of the iron F_2^{Fe} per nucleon over the deuteron F_2^d. This effect, the EMC effect, was confirmed in a subsequent analysis of old SLAC data [15], and an extensive study, using different nuclear targets, provided the exact x behavior of the effect versus the mass number A of nuclei [16]. The SLAC experimental data are shown in Figure 2 and indeed indicate a significant x and A dependence for the inelastic cross section ratio $(\sigma^A/\sigma^d)_{is}$ for several nuclei from ^{4}He to Au. The σ^A and deuteron σ^d cross sections are per nucleon and the ratio has been adjusted for an isoscalar nucleus of mass number A. This cross section ratio is equal to the equivalent isoscalar structure function ratio $(F_2^A/F_2^d)_{is}$.

2 Theory Overview

The F_2^n/F_2^p ratio can be calculated in a number of models of the nucleon. In a world of exact SU(6) symmetry, the wave function of a proton, polarized in the $+z$ direction for instance, would be simply [7]:

$$\begin{aligned} p\uparrow \; = \; & \frac{1}{\sqrt{2}} u\uparrow (ud)_{S=0} + \frac{1}{\sqrt{18}} u\uparrow (ud)_{S=1} - \frac{1}{3} u\downarrow (ud)_{S=1} \\ & - \frac{1}{3} d\uparrow (uu)_{S=1} - \frac{\sqrt{2}}{3} d\downarrow (uu)_{S=1} \; , \end{aligned} \tag{8}$$

where the subscript S denotes the total spin of the "diquark" partner of the quark. In this limit, the u and d quarks in the proton would be identical, and the nucleon and Δ isobar would, for example, be degenerate in mass. In deep-inelastic scattering, exact SU(6) symmetry would be manifested in equivalent shapes for the valence quark distributions of the proton, which would be related simply by $u_v(x) = 2d_v(x)$ for all x. For the neutron to proton F_2 structure function ratio this would imply [17]:

$$\frac{F_2^n}{F_2^p} = \frac{2}{3}, \qquad \frac{d}{u} = \frac{1}{2} \qquad \text{[SU(6) symmetry]}. \tag{9}$$

In nature, spin-flavor SU(6) symmetry is, of course, broken. The nucleon and Δ masses are split by some 300 MeV. In deep inelastic scattering off the nucleon, this symmetry breaking is reflected in the experimental observation that the d quark distribution is softer than the u quark distribution, with the F_2^n/F_2^p ratio deviating from the SU(6) expectation. The correlation between the mass splitting in the **56** baryons and the large-x behavior of

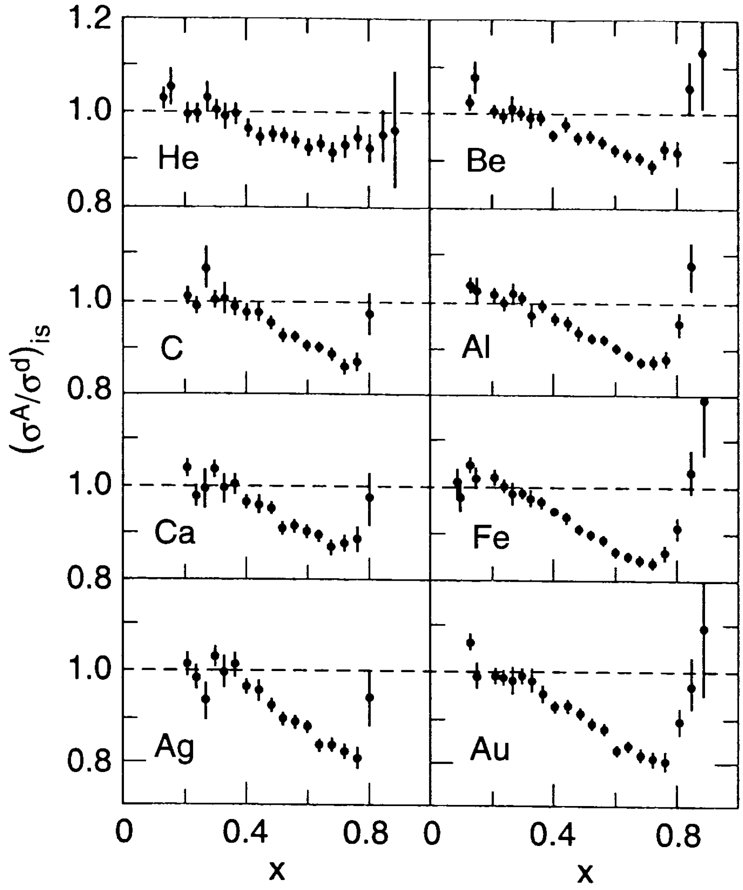

Figure 2: SLAC data on the inelastic cross section ratio of several nuclei (σ^A) to deuterium (σ^d) versus the Bjorken x [16]. The cross sections are per nucleon and the ratio has been adjusted for an isoscalar nucleus of mass number A.

F_2^n/F_2^p was observed some time ago by Close [18] and Carlitz [19]. Based on phenomenological [18] and Regge [19] arguments, the breaking of the symmetry in Equation 8 was argued to arise from a suppression of the "diquark" configurations having $S = 1$ relative to the $S = 0$ configuration as $x \to 1$. Such a suppression is in fact quite natural if one observes that whatever mechanism leads to the observed $N - \Delta$ splitting (e.g. color-magnetic force, instanton-induced interaction, pion exchange), it necessarily acts to produce a mass splitting between the two possible spin states of the two quarks which act as spectators to the hard collision, $(qq)_S$, with the $S = 1$ state heavier than the $S = 0$ state by some 200 MeV [20]. From Equation 8, a dominant scalar valence diquark component of the proton suggests that in the $x \to 1$ limit, F_2^p is essentially given by a single quark distribution (i.e. the u), in which case:

$$\frac{F_2^n}{F_2^p} \to \frac{1}{4}, \qquad \frac{d}{u} \to 0 \qquad [S = 0 \text{ dominance}]. \tag{10}$$

This expectation has, in fact, been built into most phenomenological fits to the parton distribution data [21, 22, 23, 24].

The phenomenological suppression of the d quark distribution can be understood within the hyperfine-perturbed quark model of Isgur *et al.* [25, 26]. The color hyperfine interaction is generated by one-gluon exchange between quarks in the core. At lowest order, the Hamiltonian for the color-magnetic hyperfine interaction between two quarks is proportional to $\vec{S}_i \cdot \vec{S}_j$, where $\vec{S}_i$ is the spin vector of quark i. Because this force is repulsive if the spins of the quarks are parallel and attractive if they are antiparallel, from the SU(6) wave function in Equation 8 it naturally leads to an increase in the mass of the Δ and a lowering of the mass of the nucleon, and a softening of the d quark distribution relative to the u [26].

An alternative suggestion, based on a perturbative QCD argument, was originally formulated by Farrar and Jackson [27]. There it was shown that the exchange of longitudinal gluons, which are the only type permitted when the spins of the two quarks in $(qq)_S$ are aligned, would introduce a factor $(1-x)^{1/2}$ into the Compton amplitude — in comparison with the exchange of a transverse gluon between quarks with spins anti-aligned. In this approach, the relevant component of the proton valence wave function at large x is that associated with states in which the total "diquark" spin projection, S_z, is zero as $x \to 1$. Consequently, scattering from a quark polarized in the opposite direction to the proton polarization is suppressed by a factor $(1-x)$ relative to the helicity-aligned configuration.

A similar result is also obtained in the treatment of Brodsky *et al.* [28] (based on quark-counting rules), where the large-x behavior of the parton distribution for a quark polarized parallel ($\Delta S_z = 1$) or antiparallel ($\Delta S_z = 0$) to the proton helicity is given by: $q^{\uparrow\downarrow}(x) = (1-x)^{2n-1+\Delta S_z}$, where n is the minimum number of non-interacting quarks (equal to 2 for the valence quark distributions). Using Equation 8, in the $x \to 1$ limit one therefore predicts:

$$\frac{F_2^n}{F_2^p} \to \frac{3}{7}, \qquad \frac{d}{u} \to \frac{1}{5} \qquad [S_z = 0 \text{ dominance}]. \tag{11}$$

It should be noted that in the latter two treatments, the d/u ratio does not vanish as $x \to 1$ and the F_2^n/F_2^p ratio tends to 3/7 instead of 1/4.

Moving to the EMC effect, despite the intense theoretical work over the 20 years since its discovery, there is no unique theory or universally accepted model that describes its origin. There are many classes of models offering possible explanations of the effect. One class tries to explain the effect by revisiting the bound-nucleon problem and offering refined treatments for the nuclear binding and nucleon off-shellness. A second class attributes the existence of the effect to a possible increasing enhancement of the pion field, associated with the nucleon-nucleon interaction, with the nuclear mass number A. A third class departs from the conventional meson-nucleon framework of the nucleus and assumes that a dense nucleus with tightly packed nucleons has to be viewed and treated as a collection of multi-quark clusters. A distinct model in this class is one offering a quark-diquark structure of the nucleon, with the diquark modified in the nuclear medium. A fourth class is based on the idea of dynamical rescaling arising from the observation that iron F_2 structure function data resemble deuterium F_2 structure function data of higher Q^2 values. The underlying physical idea in this rescaling model is the change in the quark confinement scale of a nucleon embedded in a nucleus.

The above four classes are sometimes complemented by additional mechanisms that can offer explanations for the EMC effect pattern in specific x regions, like the well known shadowing mechanism, which reproduces the low-x pattern of the effect, and the increased Fermi momentum of the nucleons in heavier nuclei, which accounts for the large-x behavior of the EMC ratio data. The large number of approaches and models trying to explain the effect as well as comprehensive detailed accounts and comparisons of theoretical calculations with data are given in the excellent reviews of References [29, 30].

It is widely accepted that the first step in the understanding of the origin of the EMC effect is a realistic calculation of the structure function F_2 of the light, simplest nuclei in nature and in particular of the $A = 3$ mirror nuclei: ^{3}He and ^{3}H. Of paramount importance would be a comparison of theory and experimental data for the ratio of the structure functions of the two nuclei, where both systematic and theoretical inherent uncertainties cancel out, making this ratio a benchmark for the understanding of the EMC effect [31].

3 Motivation for a New Experiment

Although the problem of extracting neutron structure functions from deuterium data is rather old [32], the discussion has been recently revived [33, 34, 35] with the realization [36] that F_2^n, extracted from F_2^p and F_2^d by taking into account Fermi-motion *and* binding effects in deuterium, could be significantly larger [34, 36] than that extracted in earlier analyses [12] in which only Fermi-motion corrections were applied.

Melnitchouk and Thomas [34] have incorporated binding and off-shell effects within a covariant framework in terms of relativistic deuteron wave functions (as calculated by Gross and collaborators [37], for instance). Neglecting the relativistic deuteron P-states and off-shell deformation of the bound nucleon structure function (which were found to contribute at the $\sim 1\%$ level [38]), the deuteron F_2^d structure function can be written as a convolution of the free proton and neutron F_2 structure functions and a nucleon momentum distribution in the deuteron, $f_{N/d}$:

$$F_2^d(x,Q^2) = \int dy \; f_{N/d}(y) \; [F_2^p(x/y,Q^2) + F_2^n(x/y,Q^2)], \tag{12}$$

where y is the fraction of the 'plus'-component of the nuclear momentum carried by the interacting nucleon, and $f_{N/d}(y)$ takes into account both Fermi-motion and binding effects. Their reanalysis of the SLAC data based upon this improved theoretical treatment led to larger F_2^n/F_2^p values as compared with the Fermi-motion only extracted values. As can be seen in Figure 3, the difference at $x = 0.85$ can be up to $\sim 50\%$.

Whitlow *et al.* [36] incorporated binding effects using the "nuclear density model" of Frankfurt and Strikman [39]. In this model, the EMC effect for the deuteron scales with nuclear density as for heavy nuclei:

$$\frac{F_2^d}{F_2^p + F_2^n} = 1 + \frac{\rho_d}{\rho_A - \rho_d}\left[\frac{F_2^A}{F_2^d} - 1\right] \;, \tag{13}$$

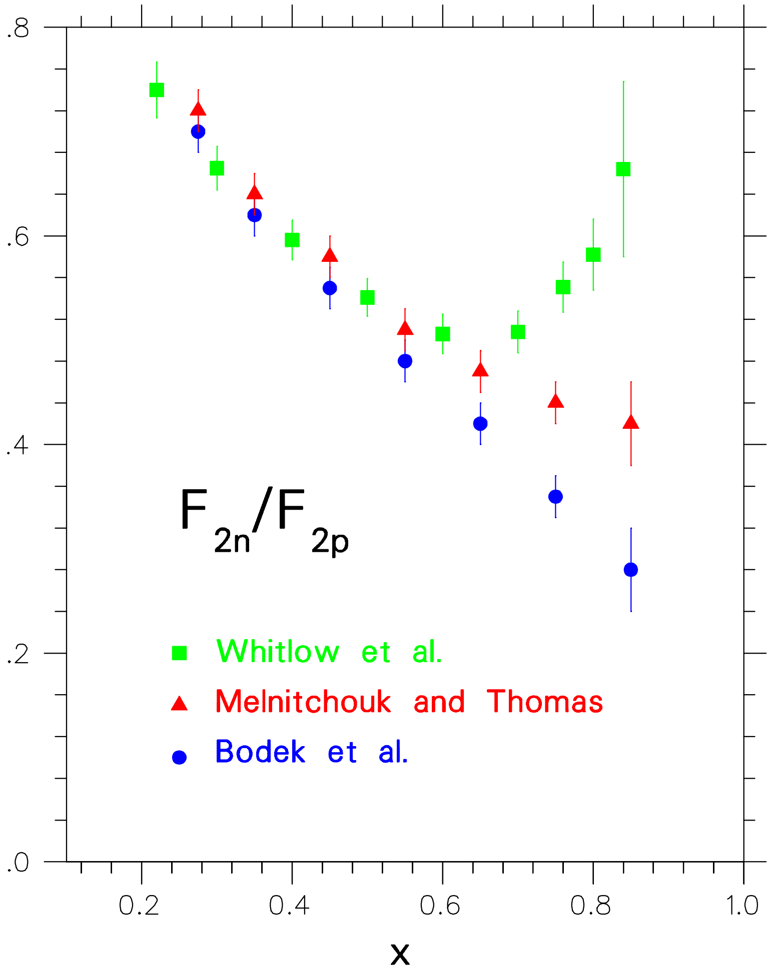

Figure 3: The F_2^n/F_2^p ratio extracted from proton and deuteron DIS measurements [11] with a) a Fermi-smearing model (Bodek *et al.* [12]), b) a covariant model that includes binding and off-shell effects (Melnitchouk and Thomas [34]), and c) the "nuclear density model" that also incorporates binding and off-shell effects (Frankfurt and Strikman [36, 35, 39]).

where ρ_d is the deuteron charge density, and ρ_A and F_2^A refer to a heavy nucleus with mass number A. This model predicts F_2^n/F_2^p values that are significantly higher ($> 100\%$) than the Fermi-motion only extracted ones at high x, as can be seen in Figure 3.

It is evident from the above two models that neglecting nuclear binding effects in the deuteron can introduce, at large x, a significant uncertainty in the extraction of the F_2^n/F_2^p and d/u ratios. A typical example for the magnitude of the uncertainty for the d/u ratio,

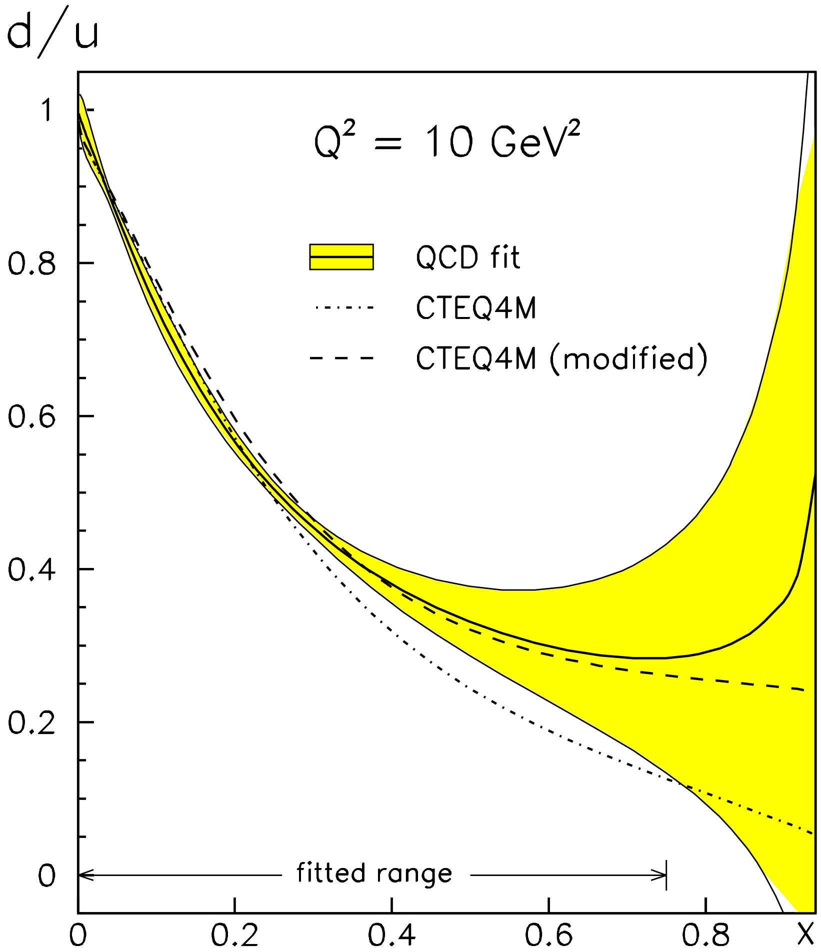

Figure 4: A typical uncertainty in the determination of the quark d/u distribution ratio by the QCD fit of Botje [40] on DIS cross section data. The solid curve is a QCD fit, and the shaded area shows the uncertainty in the fit. The dot-dashed curve represents the standard CTEQ4 fit [41], while the dashed curve corresponds to the CTEQ4 fit with a modified d quark distribution with $d/u \to\approx 0.2$ as $x \to 1$.

as estimated by one calculation from a QCD fit of proton and deuteron structure function data, is given in Figure 4 [40]. In the absence of experimental data or a unique theory for the magnitude of binding effects and the existence of the EMC effect in the deuteron, the question of the large-x behavior of F_2^n/F_2^p and d/u can only be settled by a measurement which does not rely on the use of the deuteron as an effective neutron target.

The above situation can be remedied by using a method proposed by Afnan *et al.* [42, 43], which maximally exploits the mirror symmetry of $A = 3$ nuclei and extracts the F_2^n/F_2^p ratio from DIS measurements off ^{3}H and ^{3}He. Regardless of the absolute values of the nuclear EMC effects in ^{3}He or ^{3}H, the differences between these will be small – on the scale of charge symmetry breaking in the nucleus – which allows for a determination of the F_2^n/F_2^p and d/u ratios at large-x values essentially free of nuclear contamination. At the same time, precise DIS measurements off ^{3}H and ^{3}He will provide the necessary structure function F_2 data for detailed studies of the EMC effect, which could lead to a canonical theory for the explanation of its dynamical origin. In summary, this method will, as it has been stated in Reference [31], i) unambiguously determine the valence u and d quark distributions of the free nucleon, ii) complete our knowledge of the EMC effect over the full range of nuclear mass number by determining the effect in the three-body systems and in the deuteron, and iii) provide valuable input in sorting out the change of the nucleon structure in the nuclear medium, which is fundamental to our understanding of QCD itself.

4 Exploring Deep Inelastic Scattering off ^{3}H and ^{3}He

In the absence of a Coulomb interaction and in an isospin symmetric world, the properties of a proton (neutron) bound in the ^{3}He nucleus would be identical to that of a neutron (proton) bound in the ^{3}H nucleus. If, in addition, the proton and neutron distributions in ^{3}He (and in ^{3}H) were identical, the neutron structure function could be extracted with no nuclear corrections, regardless of the size of the EMC effect in ^{3}He or ^{3}H separately.

In practice, ^{3}He and ^{3}H are of course not perfect mirror nuclei – their binding energies for instance differ by some 10% – and the proton and neutron distributions are not quite identical. However, the $A = 3$ system has been studied for many years, and modern realistic $A = 3$ wave functions are known to rather good accuracy. In a self-consistent framework one can use the same nucleon-nucleon (NN) interaction which describes the two-nucleon system to provide the basic input interaction into the three-nucleon calculation. Therefore, the wave functions can be tested against a large array of observables which put rather strong constraints on the models.

Defining the EMC-type ratios for the F_2 structure functions of ^{3}He and ^{3}H (weighted by corresponding isospin factors) by:

$$R({}^3\mathrm{He}) = \frac{F_2^{{}^3\mathrm{He}}}{2F_2^p + F_2^n}\ , \qquad R({}^3\mathrm{H}) = \frac{F_2^{{}^3\mathrm{H}}}{F_2^p + 2F_2^n}\ , \tag{14}$$

one can write the "super-ratio", $\mathcal{R}$, of these as:

$$\mathcal{R} \ = \ \frac{R({}^3\mathrm{He})}{R({}^3\mathrm{H})}\ . \tag{15}$$

Inverting this expression directly yields the ratio of the free neutron to proton structure functions:

$$\frac{F_2^n}{F_2^p} \ = \ \frac{2\mathcal{R} - F_2^{{}^3\mathrm{He}}/F_2^{{}^3\mathrm{H}}}{2F_2^{{}^3\mathrm{He}}/F_2^{{}^3\mathrm{H}} - \mathcal{R}}\ . \tag{16}$$

We stress that F_2^n/F_2^p extracted via Equation 16 does not depend on the size of the EMC effect in ^{3}He or ^{3}H, but rather on the *ratio* of the EMC effects in ^{3}He and ^{3}H. If the neutron and proton distributions in the $A = 3$ nuclei are not dramatically different, one might expect $\mathcal{R} \approx 1$. To test whether this is indeed the case requires an explicit calculation of the EMC effect in the $A = 3$ system.

The conventional approach employed in calculating nuclear structure functions in the valence quark region, $x > 0.3$, is the impulse approximation, in which the virtual photon, γ^*, mediating the electron-nucleus interaction, scatters incoherently from individual nucleons in the nucleus [29]. The nuclear cross section is determined by factorizing the γ^*–nucleus interaction into γ^*–nucleon and nucleon–nucleus amplitudes. The structure function of a nucleus, F_2^A, can then be calculated by folding the nucleon structure function, F_2^N, with the nucleon momentum distribution in the nucleus, $f_{N/A}$, as in Equation 12:

$$F_2^A(x) \ = \ \int dy\ f_{N/A}(y)\ F_2^N(x/y) \ \equiv \ f_{N/A}(x) \otimes F_2^N(x)\ , \tag{17}$$

where the Q^2 dependence in the structure functions is implicit. The convolution expression in Equation 17 is correct in the limit of large Q^2; at finite Q^2 there are additional contributions to F_2^A from the nucleon F_1^N structure functions, although these are suppressed by powers of M^2/Q^2. Corrections to the impulse approximation appear in the guise of final state interactions, multiple rescattering (nuclear shadowing), NN correlations and 6-quark

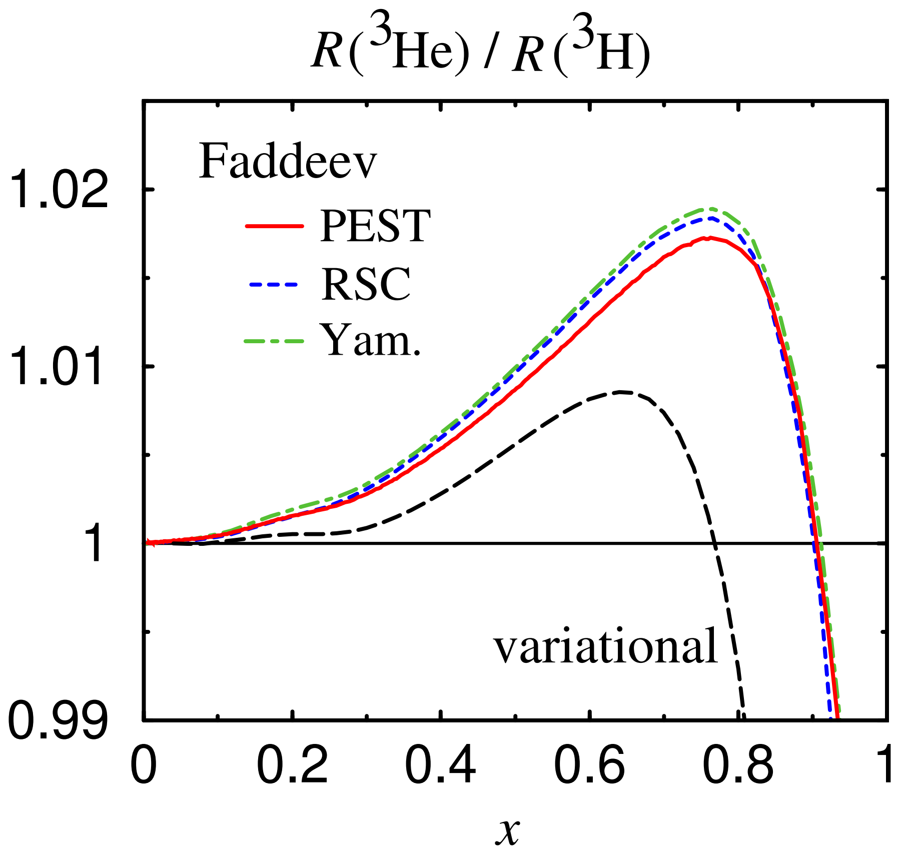

Figure 5: The "super-ratio" $\mathcal{R}$ of nuclear EMC ratios for ^{3}He and ^{3}H nuclei, with the nucleon momentum distribution calculated from the Faddeev (PEST, RSC, Yamaguchi) and variational (RSC) wave functions [43].

clusters, however, these are generally confined to either the small-x [44], or very large-x ($x > 0.9$) [45] regions.

The distribution $f(y)$ of nucleons in the nucleus is related to the nucleon spectral function $S(p)$ by [29]:

$$f(y) = \int d^3\vec{p} \left(1 + \frac{p_z}{p_0}\right) \delta\left(y - \frac{p_0 + p_z}{M}\right) S(p) \ , \tag{18}$$

where p is the momentum of the bound nucleon. For an $A = 3$ nucleus the spectral function is evaluated from the three-body nuclear wave function, calculated by either solving the homogeneous Faddeev equation with a given two-body interaction [42, 46] or by using a variational technique [47]. The model dependence of the distribution function can be examined by using several different potentials. In Refs. [42, 43] a number of potentials were used, including the "EST" (Ernst-Shakin-Thaler) separable approximation to the Paris potential [48] [referred to as "Paris (EST)"], the unitary pole approximation [49] to the Reid Soft Core (RSC) potential, and the Yamaguchi potential [50] with 7% mixing between $^3S_1$ and $^3D_1$ waves. The Argonne AV18 potential [52] was also used for the calculations in Refs. [51, 53].

In terms of the proton and neutron momentum distributions, the F_2 structure function for ^{3}He is given by:

$$F_2^{^3\mathrm{He}} = 2\, f_{p/^3\mathrm{He}} \otimes F_2^p + f_{n/^3\mathrm{He}} \otimes F_2^n \,. \tag{19}$$

Similarly for ^{3}H, the structure function is evaluated from the proton and neutron momentum distributions in ^{3}H:

$$F_2^{^3\mathrm{H}} = f_{p/^3\mathrm{H}} \otimes F_2^p + 2\, f_{n/^3\mathrm{H}} \otimes F_2^n \,. \tag{20}$$

Because isospin symmetry breaking effects in nuclei are quite small, one can to a good approximation relate the proton and neutron distributions in ^{3}He to those in ^{3}H:

$$f_{n/^3\mathrm{H}} \approx f_{p/^3\mathrm{He}} \,, \qquad f_{p/^3\mathrm{H}} \approx f_{n/^3\mathrm{He}} \,, \tag{21}$$

although in practice both the isospin symmetric and isospin symmetry breaking cases have been considered explicitly. Note that even in the isospin symmetric case the proton and neutron distributions in ^{3}He will be different because while the neutron in ^{3}He is accompanied by a spectator pp, the spectator system of the proton is either an uncorrelated pn pair or a recoiling deuteron.

The ratio $\mathcal{R}$ of EMC ratios for ^{3}He and ^{3}H, as calculated by Afnan *et al.* [42, 43] is shown in Figure 5 for the various nuclear model wave functions [Paris (EST), RSC and Yamaguchi], using the CTEQ parametrization [24] of parton distributions at $Q^2 = 10$ (GeV/c)^2 for F_2^N. The EMC effects are seen to largely cancel over a large range of x, out to $x \sim 0.9$, with the deviation from unity of less than 2%. Furthermore, the dependence on the nuclear wave function is very weak. The pattern of behavior of the ratio $\mathcal{R}$ has been confirmed in independent calculations by Pace *et al.* [51], using a variational approach to calculate the

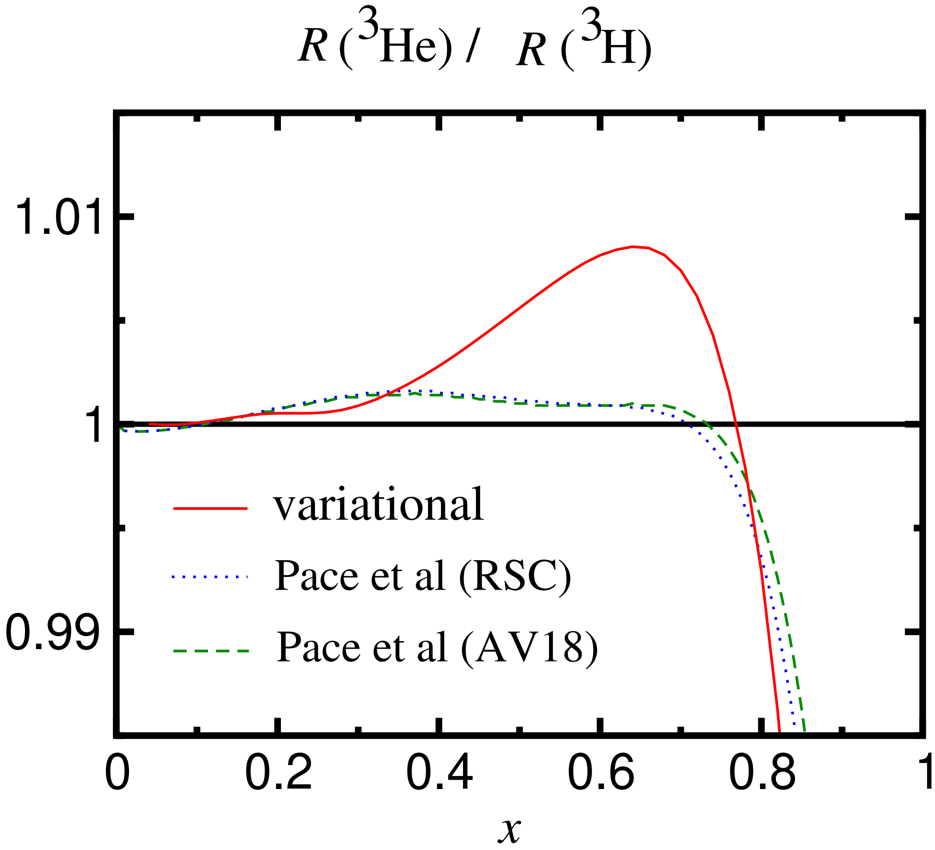

Figure 6: Ratio of nuclear EMC ratios for ^{3}He and ^{3}H for the variational calculation [43] (solid) and from Ref. [51] for the RSC (dotted) and AV18 (dashed) NN potentials (see text).

three-body spectral function, and by Sargsian *et al.* [53] using the Green function Monte Carlo wave functions from Ref. [52].

As seen in Figure 6, the deviation of $\mathcal{R}$ from unity is also well within the 2% range for both of the above cases. Note that the solid curve (from the work of Ciofi degli Atti and Liuti [54]) is computed using the RSC NN potential with the CTEQ parametrization of the nucleon structure function, while the dashed and dot-dashed curves (from Pace *et al.* [51]) use the RSC and AV18 potentials with the structure function fits from Ref. [55].

The dependence of $\mathcal{R}$ on the input nucleon structure function parametrization is illustrated in Figure 7, where several representative curves at $Q^2 = 10$ (GeV/c)^2 are given: apart from the standard CTEQ fit (solid), the results for the GRV [56] (dot-dashed), Donnachie-

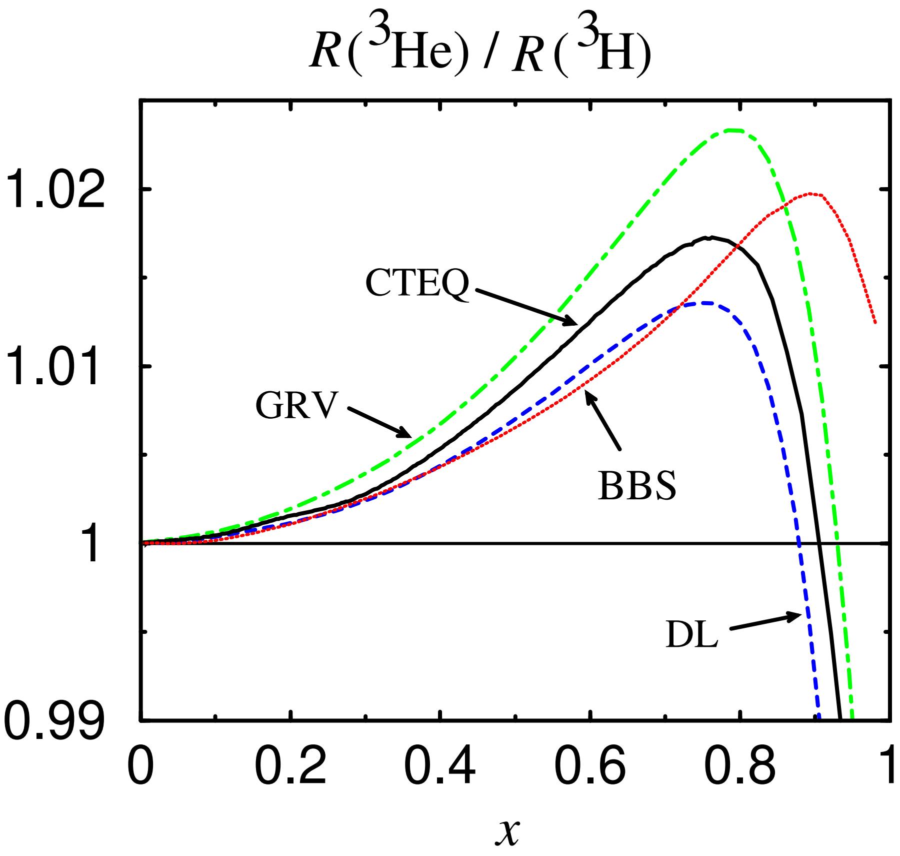

Figure 7: Ratio of nuclear EMC ratios for ^{3}He and ^{3}H with the Paris (EST) wave functions, using various nucleon structure function parametrizations [42] (see text): CTEQ (solid), GRV (dot-dashed), BBS (dotted), and DL (dashed).

Landshoff (DL) [57] (dashed), and BBS [28] (dotted) parametrizations are also shown (the latter at $Q^2 = 4$ (GeV/c)^2). For $x < 0.6$ there is little dependence ($< 0.5\%$) in the ratio on the structure function input. For $0.6 < x < 0.85$ the dependence is greater, but still with $< \pm 1\%$ deviation away from the central value $\mathcal{R} = 1.01$. The spread in this region is due mainly to the poor knowledge of the neutron structure function at large x. Beyond $x \approx 0.85$ there are few data in the deep-inelastic region on either the neutron or the proton structure functions, so here both the d and u quark distributions are poorly determined.

Despite the seemingly strong dependence on the nucleon structure function input at very large x, this dependence is actually artificial. In practice, once the ratio $F_2^{^3\mathrm{He}}/F_2^{^3\mathrm{H}}$ is measured, one can employ an iterative procedure to eliminate this dependence altogether. Namely, after extracting F_2^n/F_2^p from the data using some calculated $\mathcal{R}$, the extracted F_2^n can then be used to compute a new $\mathcal{R}$, which is then used to extract a new and better value of F_2^n/F_2^p. This procedure is iterated until convergence is achieved and a self-consistent solution for the extracted F_2^n/F_2^p is obtained. Both Afnan *et al.* [42] and Pace *et al.* [51] have independently confirmed the convergence of this procedure.

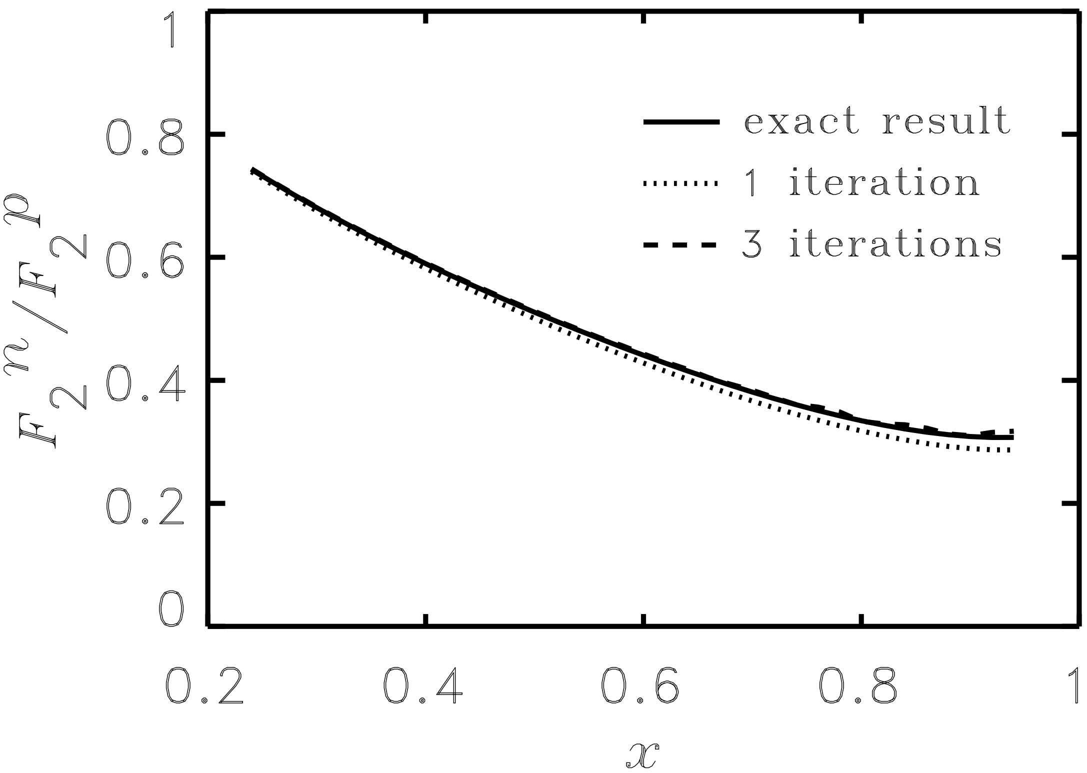

Figure 8: The convergence of the iterative procedure which eliminates the nucleon structure function dependence in the F_2^n/F_2^p extraction, from Ref. [43]. The input is $F_2^n/F_2^p = 1$, and the ratio after ~ 3 iterations is indistinguishable from the exact result (solid).

As an illustration, we show in Figure 8 the result from Afnan *et al.* [43] for different numbers of iterations using as input $F_2^n/F_2^p = 1$. The convergence is relatively rapid — by the third iteration the extracted function is almost indistinguishable from the exact result. Although the effect on $\mathcal{R}$ from the present lack of knowledge of the nucleon structure function is $< 2\%$ for $x < 0.85$, this uncertainty can in principle be eliminated altogether via iteration, so that the only model dependence of $\mathcal{R}$ will be from the nuclear interaction in the $A = 3$ nucleus.

Of course the accuracy of the iteration procedure is only as good as the reliability of the above formalism and wave functions used to calculate the nuclear structure functions allows. The ratios in Figure 5 were calculated using three-nucleon wave functions neglecting the Coulomb interaction and working in an isospin basis (possible three-body forces can be omitted since these are expected to have a negligible effect on $\mathcal{R}$). To estimate the effect of neglecting the Coulomb interaction in ^{3}He and at the same time correct the long-range part of the three-body wave function due to the change in the binding energy, Afnan *et al.* [43] have modified the $^1S_0$ potential in ^{3}He and ^{3}H to reproduce their respective experimental energies. In this way the $^3S_1 -^3 D_1$ interaction responsible for the formation of the deuteron is unchanged. This approximation spreads the effect of the Coulomb interaction over both the *pp* and *np* interaction in the ^{1}S$_0$ channel, and to this extent, it shifts some of the Coulomb effects in the neutron distribution in ^{3}He to the proton distribution. However, this simple modification to the $^1S_0$ interaction allows one to study explicitly the possible effects associated with the differences in the binding energies of ^{3}He and ^{3}H.

The ratio $\mathcal{R}$ calculated in Ref. [43] with the Paris (EST) wave function modified according to this prescription is shown in Figure 9, labeled "Paris (EST)*" [the CTEQ parametrization of the nucleon structure function at $Q^2 = 10$ (GeV/c)^2 is used]. The result of this modification is a shift of $< 0.5\%$ in $\mathcal{R}$, with the net effect still being a ratio which deviates by $< 2\%$ from unity.

There are a number of other possible effects which could influence the ratio $\mathcal{R}$, not included in the formalism of Equation 17, and which have been considered in Refs. [43, 53]. The derivation of the convolution approximation in Equation 17 assumes that the nucleon off-shell dependence in the bound nucleon structure function is negligible. The off-shell dependence of F_2^N is, as a matter of principle, not measurable, since one can always redefine the nuclear spectral function to absorb any p^2 dependence in the bound nucleon structure function. However, off-shell effects can be identified once a particular form of the interaction of a nucleon with the surrounding nuclear medium is specified. The discussion of off-shell

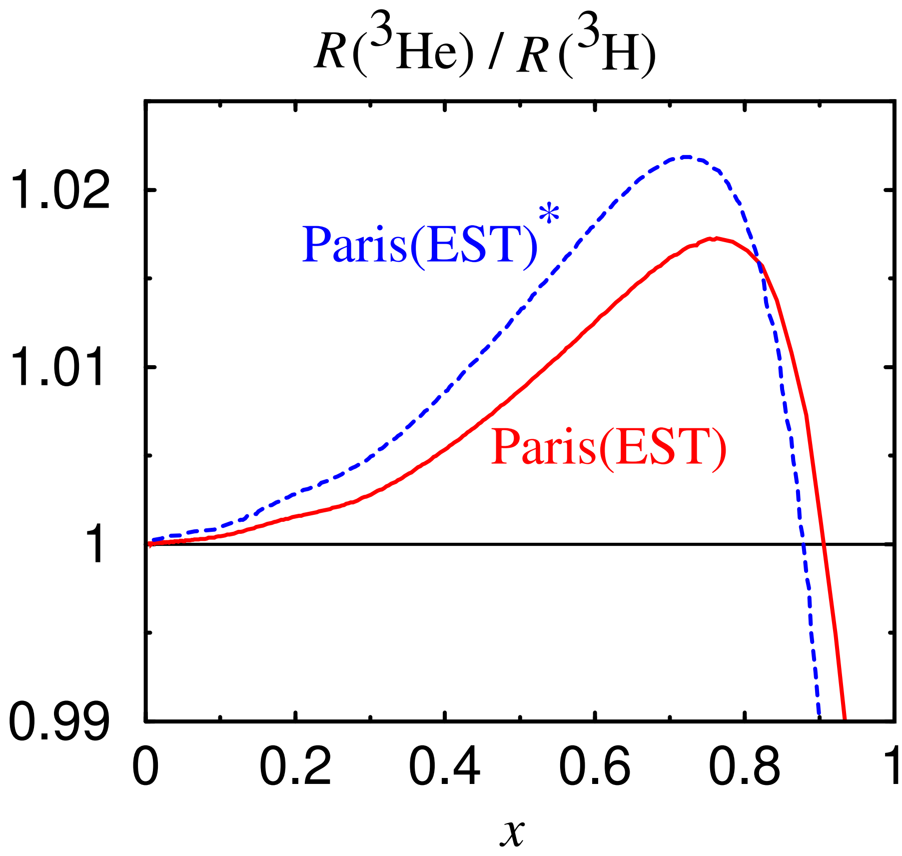

Figure 9: Ratio of nuclear EMC ratios for ^{3}He and ^{3}H for the Paris (EST) model (solid) and for the modified Paris (EST)* model (dashed) which includes explicit isospin symmetry breaking [42].

modification of the nucleon structure function in the nuclear medium is therefore understood to be within the framework of the nuclear spectral functions defined in Equation 18.

Taking the nucleon's off-shellness into account, the bound nucleon structure function in Equation 17 can be generalized to [58, 59, 60]:

$$F_2^A(x, Q^2) \;\; = \;\; \int dy \int dp^2 \; \varphi(y, p^2, Q^2) \; F_2^N(x', p^2, Q^2) \; , \tag{22}$$

where $x' = x/y$ and the function $\varphi(y, p^2, Q^2)$ depends on the nuclear wave functions. In the absence of p^2 dependence in F_2^N, the light-cone momentum distribution $f(y, Q^2)$ in Equation 17 would correspond to the p^2 integral of $\varphi(y, p^2, Q^2)$. In the approach of Ref. [58], the medium-modified nucleon structure function $F_2^N(x', p^2, Q^2)$ can be evaluated in terms of a relativistic quark spectral function which depends on the virtualities of the struck quark, k^2, and spectator system. The dependence of $k_{\min}$ on p^2 ($\neq M^2$) generates an off-shell correction which grows with A due to the A-dependence of the virtuality p^2 of the bound nucleon. This serves to enhance the EMC effect at large x in comparison with naive binding model calculations which do not take into account nucleon off-shell effects.

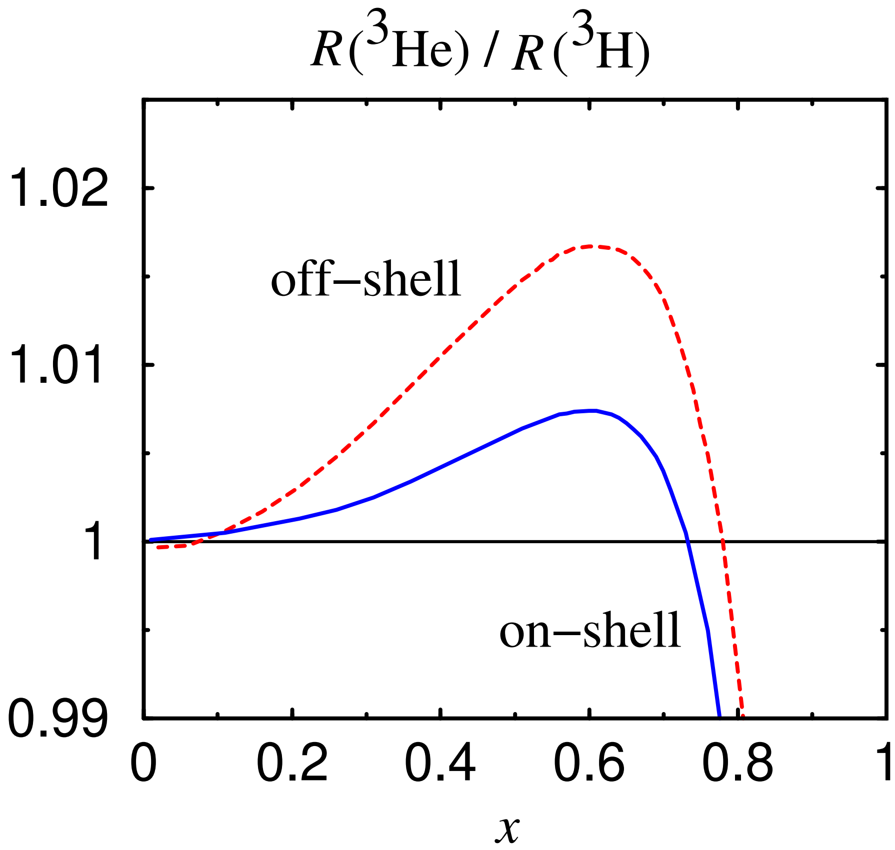

Figure 10: Ratio $\mathcal{R}$ of nuclear EMC ratios for ^{3}He and ^{3}H nuclei, with (dashed) and without (solid) nucleon off-shell corrections [58] (see text), for the variational (RSC) wave function.

The effect of the off-shell correction on the ratio $\mathcal{R}$, illustrated in Figure 10, is a small ($< 1\%$) increase in the ratio at $x \sim 0.6$. Off-shell effects of this magnitude can be expected in models of the EMC effect where the overall modification of the nuclear structure function arises from a combination of conventional nuclear physics phenomena associated with nuclear binding, and a small medium dependence of the nucleon's intrinsic structure. Other models of the EMC effect, such as the color screening model for the suppression of point-like configurations (PLC) in bound nucleons [61], attribute most or all of the EMC effect to a medium modification of the internal structure of the bound nucleon, and consequently predict larger deviations of $\mathcal{R}$ from unity [53]. However, recent ^{4}He($\vec{e}, e'\vec{p}$) polarization transfer experiments [62] indicate that the magnitude of the off-shell deformation is indeed rather small. The measured ratio of transverse to longitudinal polarization of the ejected protons in these experiments can be related to the medium modification of the electric to magnetic elastic form factor ratio. Using model independent relations derived from quark-hadron duality, the medium modifications in the form factors were related to a modification at large x of the deep inelastic structure function of the bound nucleon in Ref. [63]. In ^{4}He, for instance, the effect in the PLC suppression model was found [63] to be an order of magnitude larger than that allowed by the data [62], and with a different sign for $x > 0.65$. The results therefore place rather strong constraints on the size of the medium modification of the structure of the nucleon, suggesting little room for large off-shell corrections, and support a conventional nuclear physics description of the ^{3}He/^{3}H system as a reliable starting point for nuclear structure function calculations.

Corrections to the impulse approximation arising from the exchange of quarks between nucleons in $A = 3$ nuclei have been discussed by a number of authors [64, 65, 43, 53]. In Ref. [64] the effect on the EMC ratio, for the isospin-averaged $A = 3$ nucleus, was found to be comparable to that arising from binding. However, the analysis [64] did not allow for NN correlations, which are important at large momentum (and hence large x), so that the overall EMC effect is likely to have been overestimated. The effects of quarks which are not localized to single nucleons can alternatively be parametrized in terms of multi-quark clusters, in which six (or more) quarks form color singlets inside nuclei [66]. Six-quark configurations in the deuteron and other nuclei have been studied in a variety of observables, including nuclear electromagnetic form factors, NN scattering, as well as the EMC effect. Following Ref. [66], contributions from scattering off quarks in a six-quark cluster can be approximated by an effective six-quark structure function, $F_2^{6q}(x_{6q})$, in the nucleus, where $x_{6q} = Q^2/2M_{6q}\nu \approx x/2$. If P_{6q} is the probability of finding a six-quark cluster in the nucleus, the net effect on the ^{3}He (and similarly ^{3}H) structure function can be approximated by:

$$F_2^{^3\mathrm{He}} \longrightarrow (1 - P_{6q}) F_2^{^3\mathrm{He}} + P_{6q} F_2^{6q} \,, \tag{23}$$

where $F_2^{^3\mathrm{He}}$ is the incoherent nucleon contribution.

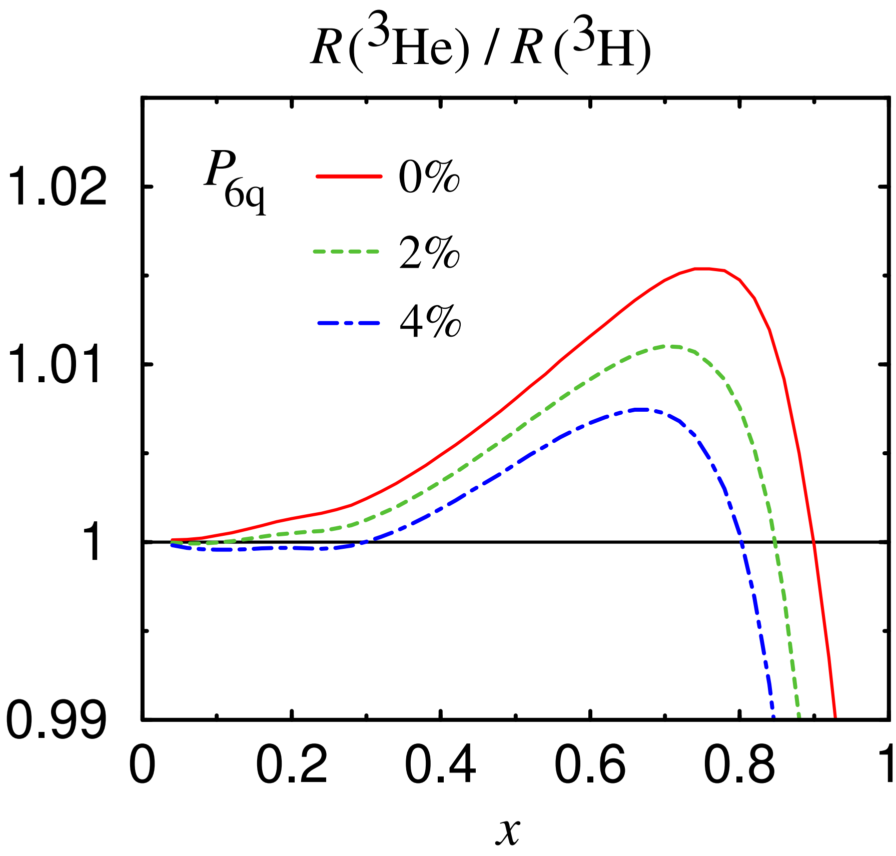

Figure 11: Ratio of nuclear EMC ratios for ^{3}He and ^{3}H for the Faddeev Paris(EST) wave function, with $P_{6q} = 0\%$, 2% and 4% six-quark configurations in the $A = 3$ wave function [43].

For a typical valence-like shape for F_2^{6q}, with the large-x behavior constrained by hadron helicity counting rules, $F_2^{6q} \sim (1 - x_{6q})^9$, Afnan *et al.* [43] have calculated the effect on $\mathcal{R}$ for $P_{6q} = 0\%$, 2% and 4%, shown in Figure 11. The overall effect is $< 1\%$ for all $x < 0.85$ even for the largest six-quark probability considered. For larger values of P_{6q} the deviation from unity is in fact even smaller, canceling some of the effects associated with nucleon off-shell dependence, for instance. Afnan *et al.* [43] and Sargsian *et al.* [53] have also considered other six-quark structure functions, and while there is some sensitivity to the exact shape of F_2^{6q}, the $\sim 1\%$ effect on $\mathcal{R}$ appears to be an approximate upper limit for all x.

The analyses of the convolution model and the various extensions discussed in Refs. [42, 43, 51, 53] demonstrate the magnitude of the theoretical uncertainty in the calculation of the ratio $\mathcal{R}$. For the purpose of this proposal we assume that we can describe $\mathcal{R}$ with a central value and assign a systematic uncertainty that grows from 0.0% at $x = 0$ to $\pm 1.0\%$ at $x = 0.8$. Further theoretical investigations in the future could possibly reduce this uncertainty.

5 The Experiment

The upgraded 6 GeV beam of the Continuous Electron Beam Accelerator of Jefferson Lab offers a unique opportunity to perform deep inelastic electron scattering off the ^{3}He and ^{3}H mirror nuclei at large-x values. The DIS cross section for ^{3}H and ^{3}He is given in terms of their F_1 and F_2 structure functions by Equation 1, where M represents in this case the nuclear mass. The nuclear structure functions F_1 and F_2 are connected through the ratio $R = \sigma_L/\sigma_T$, where σ_L and σ_T are the virtual photoabsorption cross sections for longitudinally and transversely polarized photons, by:

$$F_1 = \frac{F_2(1 + Q^2/\nu^2)}{2x(1 + R)} \ . \tag{24}$$

The ratio R has been measured to be independent of the nuclear mass number A in precise SLAC and CERN measurements using hydrogen, deuterium, iron and other nuclei (for a compilation of data see References [29, 67]).

The direct substitution of Equation (24) into Equation (1) results in the elimination of F_1 in the inelastic cross section formula:

$$\sigma = \frac{4\alpha^2 (E')^2}{Q^4} \cos^2(\frac{\theta}{2}) F_2 \left[\frac{1}{\nu} + \frac{(1 + Q^2/\nu^2)}{xM(1 + R)} \tan^2(\frac{\theta}{2}) \right]. \tag{25}$$

By performing the tritium and helium measurements under identical conditions, using the same incident beam and scattered electron detection system configurations (same E, E' and θ), and assuming that the ratio R is the same for both nuclei, the ratio of the DIS cross sections for the two nuclei will provide a direct measurement of the ratio of their F_2 structure functions:

$$\frac{\sigma(^3\mathrm{H})}{\sigma(^3\mathrm{He})} = \frac{F_2(^3\mathrm{H})}{F_2(^3\mathrm{He})}. \tag{26}$$

The key issue for this experiment will be the availability of a low-density tritium target. Tritium targets have been used in the 1980's to measure the elastic form factors of ^{3}H at Saclay [68] and MIT-Bates [69]. The Saclay target contained liquid ^{3}H at 22 K and $\sim$ 20 atm. The tritium density was 0.260 g/cm^3 at the above operating conditions and was known to $\pm$0.5% (based on actual density measurements). The activity of this target was 10,000 Ci. The MIT-Bates target contained gas ^{3}H at 45 K and 15 atm. The tritium density was, under these operating conditions, 0.028 g/cm^3 with $\sim \pm 2\%$ uncertainty (based on a Virial formalism estimation), and its activity was 145,000 Ci.

The target needed for this experiment is a 12 cm stainless steel cylindrical cell with diameter of 1.5 cm, filled at room temperature with gas tritium pressurized to 11 atm. Since high missing mass resolution is not an issue for deep inelastic scattering measurements, the target cell walls and end-caps can be sufficiently thick to assure the mechanical integrity of the cells. The tritium density would be 9.6×10^{-4} g/cm^3, resulting in a low, tolerable activity of 190 Ci. This activity is 760 times less than the Bates target activity and 110 times less than the activity of a proposed general-use target for a JLab program of elastic, inelastic and quasielastic measurements after the 12 GeV energy upgrade [70].

This low activity, room-temperature gas target eliminates the cryogenic complexity of the Bates, Saclay and general-purpose JLab targets, and simplifies the design and implementation of a necessary accident containment system. It should be noted that the Stanford HEPL experiments which measured the tritium and helium elastic form factors used safely similar cells with pressurized gas tritium and helium up to 205 atm [71]. Two similar cells will also be necessary for the ^{3}He measurements and for deuterium measurements. The deuterium measurements are highly desirable for checking the overall normalization of the cross section results and for diagnosing any scattered electron momentum and angle dependent effects. At the above proposed conditions, the three gases behave like ideal gases (to the 10^{-4} level) and their density can be known to the $\pm$0.5% level. To eliminate background electrons scattering off the end-caps of the target cells, two adjustable, properly-machined tungsten collimating slits will be mounted on the support frame of the target system, right at the side of the cells. The slits will mask the electron spectrometer from the target end-caps, and at the same time they will define the effective target length seen by the spectrometer.

The large solid angle of the Hall C High Momentum Spectrometer (HMS) or the Hall A High Resolution Spectrometer (HRS) will facilitate high-statistics DIS cross section measurements [$\pm$(0.1-0.6)%] in a large-x range as well as several valuable systematic checks. An important check would be to confirm that the ratio R is the same for ^{3}H and ^{3}He (it is known that R is the same for hydrogen, deuterium and several medium and heavy nuclei like Be, Fe etc). The performance of the above spectrometers is expected to be comparable, if not better, to that of the SLAC 8 GeV/c spectrometer that has provided precise measurements for absolute DIS cross sections, DIS cross section ratios, and differences in R for several nuclei [16, 72, 67]. The overall systematic errors for these measurements have been typically $\pm$2%, $\pm$1.0% and $\pm$0.01, respectively. A similar JLab experiment using either the HRS in Hall A or the HMS in Hall C, will produce data of the same overall systematic uncertainties.

For the primary objective of the experiment, which is measurements of cross section ratios rather than absolute cross sections, many of the experimental errors that plague absolute measurements will cancel out. The experimental uncertainties on the ratio of cross sections should be similar to those achieved by SLAC experiments E139 [16] and E140 [72, 67], which were typically $\pm$1.0%. It is a well known experimental fact that the best-determined cross sections and cross section ratios for inelastic electron scattering off nuclei have resulted from experiments using "small" solid angle traditional spectrometers like the SLAC 8 GeV/c and 20 GeV/c spectrometers. Both HMS and HRS are qualitatively similar to the SLAC spectrometers and they will provide excellent cross section data.

Inelastic scattering with the upgraded 6 GeV JLab electron beam can provide measurements of the ^{3}H and ^{3}He F_2 structure functions in the x range from 0.2 to 0.8. The electron scattering angle will range from 12° to 84° and the scattered electron energy from 0.5 to 3.8 GeV. It is assumed that either spectrometer system will be instrumented with a threshold gas Cherenkov counter and a segmented lead-glass calorimeter, which will provide discrimination between scattered electrons and an associated hadronic (mostly pion) background. The above two-counter combination has provided in the past a pion rejection factor of up to 10^5 to 1 [72] and has allowed DIS cross section measurements with negligible pion contamination up to a pion over electron ratio $\pi/e = 500$. The expected π/e ratio for this experiment has been estimated, using SLAC measurements of photon-nucleon cross sections [73], to be less than

1,000 at the highest-x kinematics. The pion contamination for a π/e ratio of 1,000 would be about 2%, which can be corrected with an estimated uncertainty of less than $\pm 0.5\%$. The expected π/e ratio is given in Table 1 (Appendix I) along with the kinematical parameters for the proposed core set of measurements of the ratio $F_2(^3\mathrm{H})/\mathrm{F}_2(^3\mathrm{He})$ from $x \approx 0.2$ up to $x \approx 0.8$.

The estimated cross sections, counting rates and the beam times required for the above measurements are given in Table 2 (Appendix II). Most inelastic measurements of the structure functions of ^{3}He, ^{3}H and deuterium will be taken at a constant $W = 2.0$ GeV and will cover the x range from 0.24 to 0.69. It will also be possible to measure the ^{3}He and ^{3}H structure functions at two higher x values: 0.73 and 0.77, with W values of 1.80 and 1.74 GeV respectively. The quantity W is the invariant mass of the final hadronic state: $W = (M^2 + 2M\nu - Q^2)^{1/2}$. These two points are slightly in the nucleon resonance region, but their Q^2 is high enough, 6.7 and 7.2 (GeV/c)^2, respectively. Earlier studies of the proton F_2^p structure function in the nucleon resonance region [74] found that Bloom-Gilman duality (equivalence of the structure function averaged over the resonance region with the deep inelastic scaling function) worked to good accuracy for Q^2 down to ~ 1 (GeV/c)^2. Phenomenological model studies [75] suggest that duality may work even better in the case of the neutron F_2^n structure function, so that for the two highest-x points the extracted F_2^n/F_2^p ratio could be interpreted in terms of the quark distribution ratio d/u. Furthermore, recent studies of ratios of nuclear cross sections at large values of x, between 0.6 and 0.8, strongly suggest that duality could be a good approximation for the highest Q^2 achievable at JLab [76]. This experiment will also be capable of checking the duality concept by measuring the helium and tritium cross sections at several selected, large-x kinematics over the nucleon resonance region (for different values of W).

The expected scattered electron counting rates have been estimated, under the assumption that $\sigma(^3He) \simeq \sigma_d + \sigma_p$ and $\sigma(^3H) \simeq 2\sigma_d - \sigma_p$, using values for the proton (F_2^p) and deuteron (F_2^d) structure functions and for the ratio R from the "global" analysis of the SLAC DIS data [36]. The rates assume a 6 msr solid angle and include, in an approximative way radiative effects (they are up to 20% for the kinematics of Table 2). It is evident from the listed rates that the proposed experiment will be able to provide very high-statistics data and perform necessary systematic studies in a very timely fashion. The required beam time for the x-scan of the helium and tritium cross sections, listed in Table 2, is 24 days for a canonical beam current of 100μA. Inelastic scattering from the deuteron, at selected kinematics (not listed in the Table), will require 2 days of beam time. Also, a minimal study on the validity of duality for the helium and tritium inelastic data will require one day of beam time.

A very important systematic check will be to confirm, at selected kinematics, the expectation that the ratio R is the same for ^{3}H and ^{3}He. The 6 GeV beam and the momentum and angular range available by the HRS or HMS system can provide measurements of R in the same x range (0.2-0.6) as in the SLAC NPAS E140X experiment [67] by means of a Rosenbluth separation versus $\epsilon = [1 + 2(1 + \nu^2/Q^2)\tan^2(\theta/2)]^{-1}$ (the degree of the longitudinal polarization of the virtual photon mediating the scattering). Our R measurements will be limited by inherent systematics uncertainties rather than, as in the SLAC case, statistical uncertainties, and will be of the same or better precision as compared to the SLAC measurements. The large ϵ range $\Delta\epsilon > 0.55$ that can be achieved in this experiment will be a decisive factor for the accuracy of these measurements. Four measurements of R at $x =$ 0.24, 0.37, 0.45 and 0.57 with $Q^2 = 1.40$, 2.15, 2.62 and 3.31 $(\mathrm{GeV}/c)^2$ and $W = 2.30$, 2.13, 2.02 and 1.84 GeV, respectively, will provide an excellent set of data for checking the universality of R and comparing with the world data. This set of measurements will require 3.6, 4.8 and 6.0 GeV beams (straight multiples of a 1.2 GeV single-pass machine configuration). The kinematics for these measurements is given in Table 3 (Appendix III), and the counting rates are given in Table 4 (Appendix IV). The required beam time for the R measurements is 3 days at the canonical beam current of 100μA.

The required precision of this experiment will necessitate very good knowledge of the spectrometer momentum acceptance. The most efficient and accurate method to accomplish this goal is to determine the spectrometer "acceptance function" by comparing deep inelastic deuterium cross section measurements from this experiment (taken with different central momentum configurations of the spectrometer) to a fit of the SLAC deuterium data, in conjunction with a reliable optics/solid angle model of the electron spectrometer. This method will require about one day of beam time. The spectrometer solid angle, the detector efficiency, and the overall integrity of the experimental apparatus and measurements can be checked by elastic electron-helium and electron-tritium scattering at low momentum transfers, where their cross sections are very well known by previous precise measurements at the Saclay Laboratory [68]. This experiment will offer also the opportunity to substantially improve the quality of the existing data for the tritium elastic form factors [77] in the kinematical range covered by the Saclay experiment, up to about Q^2=1.5 (GeV/c)^2, using 1.2, 2.4 and 3.6 GeV beams (straight multiples of a 1.2 GeV single-pass machine configuration). These improved data will be of great value for constraining recent theoretical calculations for the three-body electromagnetic form factors [78]. It is proposed to devote 4 days of beam time on these elastic measurements, bringing the total amount of time needed for this experiment to 35 days.

The $F_2(^3\mathrm{H})/\mathrm{F}_2(^3\mathrm{He})$ ratio is expected to be dominated by experimental uncertainties that do not cancel in the DIS cross section ratio of ^{3}H to ^{3}He and by the theoretical uncertainty in the calculation of the super-ratio $\mathcal{R}$. Assuming that the target densities can be known to the $\pm0.5\%$ level and that the relative difference in the ^{3}H and ^{3}He radiative corrections would be $\pm0.5\%$ as in the work of References [16, 72], the total experimental error in the the DIS cross section ratio of ^{3}H to ^{3}He should be $\sim \pm1.0\%$. Such an error is comparable to a realistic maximum theoretical uncertainty ($\sim \pm1.0\%$ in the vicinity of $x = 0.8$) in the calculation of the super-ratio $\mathcal{R}$.

6 Projected Experimental Results

The quality of the projected data on the F_2^n/F_2^p and d/u ratios is shown in Figures 12 and 13, respectively. The error bars include statistical, and experimental systematic and theoretical systematic uncertainties added in quadrature. They assume a $\pm1.0\%$ overall systematic experimental error in the measurement of the $\sigma(^3H)/\sigma(^3He)$ ratio and a theoretical uncertainty in the super-ratio $\mathcal{R}$ that increases linearly from 0.0% at $x = 0$ to $\pm1.0\%$ at $x = 0.8$. The shaded areas in Figures 12 and 13 indicate the present uncertainty, due to possible nuclear corrections, in the extraction of F_2^n/F_2^p and d/u from hydrogen and deuterium inelastic data. It is evident that the proposed experiment will be able to unquestionably distinguish

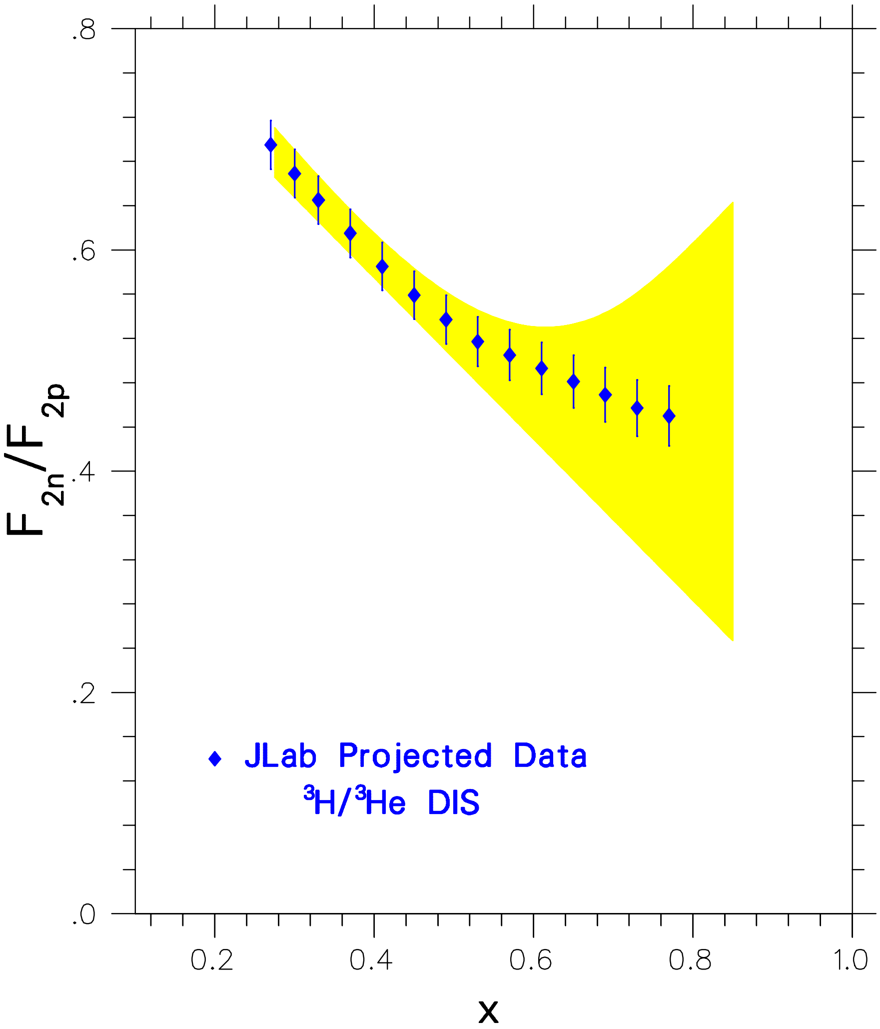

Figure 12: Projected data for the F_2^n/F_2^p structure function ratio from the proposed ^{3}H/^{3}He JLab DIS experiment. The error bars include statistical, and experimental and theoretical systematic uncertainties added in quadrature. The shaded band indicates the present uncertainty due to possible binding effects in deuteron.

between the present competing extractions of the F_2^n/F_2^p and d/u ratios from proton and deuterium DIS measurements, and to determine their values with an unprecedented precision in an almost model-independent way.

It should be noted that there is an approved Jefferson Lab experiment to extract the neutron F_2^n structure function in Hall B (BoNuS Experiment, E03-012) by measuring the

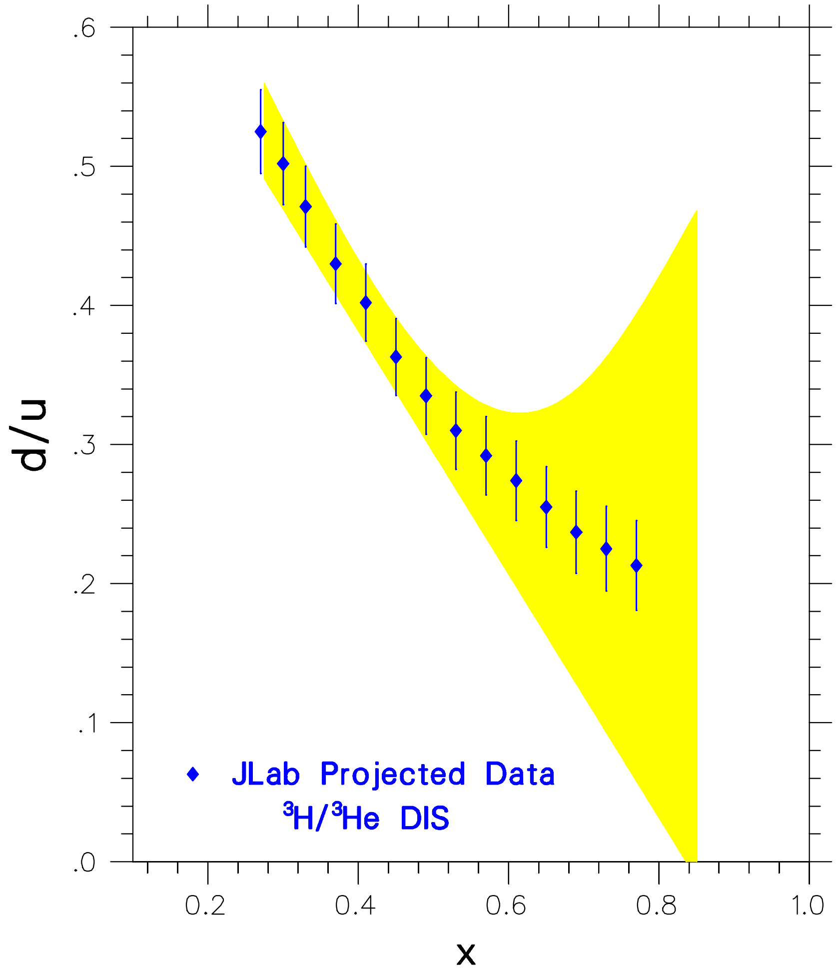

Figure 13: Projected data for the d/u quark distribution ratio from the proposed ^{3}H/^{3}He JLab DIS experiment. The error bars include statistical, and experimental and theoretical systematic uncertainties added in quadrature. The shaded band indicates the present uncertainty due to possible binding effects in deuteron. The invariant mass of the final hadronic state is $W = 2.00$ GeV for x between 0.2 and 0.7, 1.80 GeV for x=0.73 and 1.74 GeV for x=0.77. Validity of duality is assumed for the two highest x points.

cross section for semi-inclusive deep inelastic scattering off deuterium [79]. This will be accomplished by detecting backward spectator protons in coincidence with the scattered electrons from the $e + d \to e + p_s + X$ inelastic reaction. The cross section for this process is factorized in terms of the deuteron spectral function S and an effective neutron F_2 structure function:

$$\frac{d\sigma}{d^3p} \sim S(y,p^2)(F_2^n)_{eff}\left(\frac{x}{y},p^2,Q^2\right), \tag{27}$$

with:

$$y = \frac{M_d - E_s + (p_s)_z}{M_d}, \qquad p^2 = -\frac{p_t^2}{1-y} - \frac{y}{1-y}\left[M^2 - M_d^2(1-y)\right], \tag{28}$$

where p and p_s are the struck neutron and spectator proton four-momenta (with subscripts z and t denoting longitudinal and transverse components), E_s is the proton energy and M_d is the deuteron mass. This experimental approach is based on the isolation of the modifications in the structure of the bound nucleon within the impulse approximation, by choosing kinematics to minimize effects from the deuteron wave function and final-state interactions. It relies on the selection of backward low-energy proton kinematics to minimize: i) production of low-momentum protons from quark fragmentation, and ii) final-state interactions between the spectator proton and the neutron remnant. In addition, off-shell effects appear to be minimal for $p_s < 100$ MeV/c, which is expected to minimize uncertainties arising from the extrapolation of $(F_2^n)_{eff} \rightarrow (F_2^n)_{free}$. Extensive theoretical discussions of this method are given in Refs. [61, 80].

The JLab BoNuS experiment will detect scattered electrons in the CLAS detector. It will use a special thin deuterium gas target placed at the downstream end of the detector. The spectator protons will be detected in a new recoil detector (radial time projection chamber) in the backward direction. Quasi-elastic $d(e,e'p)n$ and elastic e-n scattering with spectator proton detection at low x will be also measured and used to estimate the normalization of the high-x measurements, under the assumption of no x-dependence in this normalization.

The expected statistical uncertainties on the F_2^n/F_2^p and d/u ratios are about the same for both ^{3}He/^{3}H and BoNuS experiments, and smaller than the systematic uncertainties. The projected total systematic error (experimental and theoretical) of the BoNuS experiment is, on the average, about twice as large as the projected total systematic error (experimental and theoretical) of the ^{3}He/^{3}H DIS experiment. The point-to-point total systematic error of the BoNuS experiment is, on the average (after its normalization at low x), also about twice as large as the projected point-to-point total systematic error of the ^{3}He/^{3}H DIS

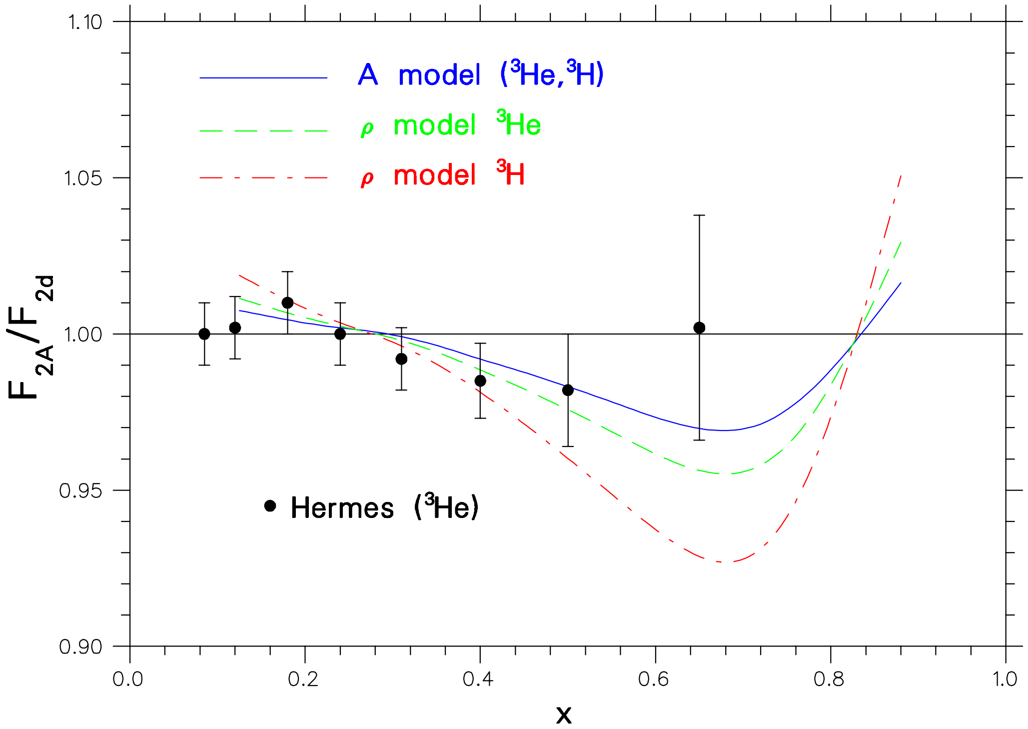

Figure 14: The ^{3}H and ^{3}He isoscalar EMC effect ratios $F_2(^3H)/F_2(d)$ and $F_2(^3He)/F_2(d)$ as predicted [16] by the nuclear mass A model (solid curve, ^{3}H and ^{3}He) and the nuclear density ρ model (dashed curve: ^{3}He, dot-dashed curve: ^{3}H). Also shown are recent data from the Hermes/DESY experiment [81].

experiment (without any normalization). Although the quality of the projected results of the ^{3}He/^{3}H DIS experiment appears to be a bit better than the BoNuS one, the two experiments are unequivocally highly complementary. Both results are expected to be pivotal for the determination of the nucleon F_2^n/F_2^p structure function and of the d/u quark distribution ratio at large values of Bjorken x.

The second goal of this $A = 3$ DIS experiment is the precise determination of the EMC effect in ^{3}H and ^{3}He. At the present time, the available SLAC and CERN data allow for two equally compatible parametrizations [16] of the EMC effect, within the achieved experimental uncertainties. In the first parametrization, the EMC effect is parametrized versus the mass number A and in the second one versus the nuclear charge density ρ. While the two parametrizations are indistinguishable for heavy nuclei, they predict quite distinct patterns for $A = 3$. This is exhibited in Figure 14, which shows the isoscalar EMC effect ratios of ^{3}H and ^{3}He. The solid curve in Figure 14 assumes that the EMC effect scales with A and describes both $A = 3$ nuclei. The dashed and dot-dashed curves assume that the EMC effect scales with ρ, applied to ^{3}He and ^{3}H, respectively. Also shown in Figure 14 are the recent DESY-Hermes data [81] on the EMC effect for ^{3}He.

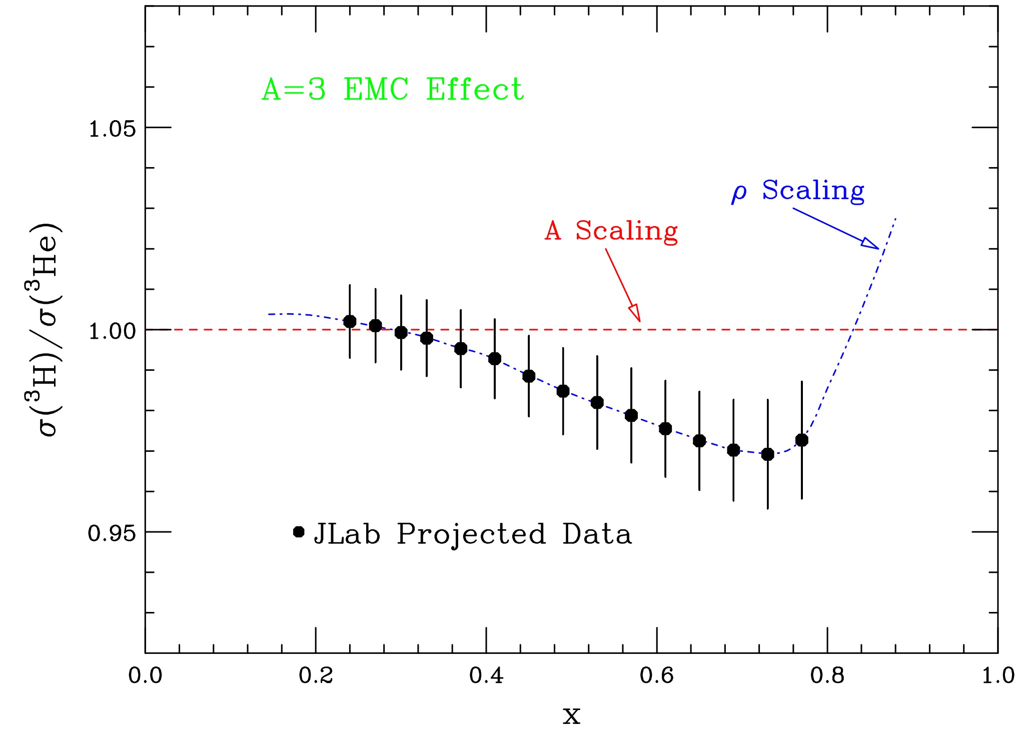

Figure 15: The ratio of the ^{3}H and ^{3}He inelastic cross sections assuming that the EMC effect scales with the nuclear mass number A (dashed curve, *i.e.*, the ratio is unity) or with nuclear charge density ρ (dot-dashed curve). Also shown are the projected data from this experiment, assuming arbitrarily that they follow the trend of the charge density parametrization of the EMC effect. The error bars include experimental systematic and statistical uncertainties added in quadrature.

The expected precision ($\pm 1\%$) of this experiment for the $F_2(^3\mathrm{H})/F_2(^3\mathrm{He})$ ratio should easily allow for distinguishing between the two competing parametrizations. This is demonstrated in Figure 15, which shows the ratio of the inelastic cross sections of the two $A = 3$

nuclei for the two parametrizations and the projected data from this experiment, assuming that they arbitrarily follow the charge density parametrization. The error bars in Figure 15 include both experimental systematic and statistical uncertainties added in quadrature. It is evident that the proposed measurements should bring a closure to the EMC effect parametrization issue and provide crucial input for a complete, consistent explanation of the origin of the EMC effect.

7 Summary

We propose to perform deep inelastic electron scattering measurements off the $A = 3$ mirror nuclei using the 6 GeV upgraded beam of CEBAF at Jefferson Lab. The experiment will require a low-density, low-activity tritium gas target as well as low-density ^{3}He and deuterium targets. It can be done in either Hall C or Hall A, using the HMS or HRS system. The required beam time is 35 days, and a sufficient amount for the check-out of the new gas target system. The measurements will determine in an almost model-independent way the fundamental F_2^n/F_2^p structure function and d/u quark distribution ratios at high Bjorken x, and distinguish between predictions based on perturbative QCD and non-perturbative models. The precision of these measurements will provide crucial input for the improvement of parton distribution parametrizations at high x, which are needed for the interpretation of high energy hadron collider data. The expected data will also test the validity of competing parametrizations of the nuclear EMC effect and provide crucial constraints on theoretical models for the explanation of its dynamical origin. This experiment offers also the opportunity to improve substantially the quality of the existing elastic electron-tritium measurements and test theoretical calculations for the three-body electromagnetic form factors.

References

[1] R. E. Taylor, Rev. Mod. Phys. **63**, 573 (1991).

[2] H. W. Kendall, Rev. Mod. Phys. **63**, 597 (1991).

[3] J. I. Friedman, Rev. Mod. Phys. **63**, 615 (1991).

[4] E. D. Bloom *et al.*, Phys. Rev. Lett. **23**, 930 (1969); M. Breidenbach *et al.*, Phys. Rev. Lett. **23**, 935 (1969).

[5] J. I. Friedman and H. W. Kendall, Annu. Rev. Nucl. Sci. **22**, 203 (1972).

[6] J. D. Bjorken, Phys. Rev. **179**, 1547 (1969); J. D. Bjorken and E. A. Paschos, Phys. Rev. **185**, 1975 (1969).

[7] F. E. Close, *An Introduction to Quarks and Partons*, Academic Press, London (1979).

[8] F.J. Yndurain, *Quantum Chromodynamics*, Springer-Verlag, Berlin (1983); T. Muta, *Foundations of Quantum Chromodynamics*, World Scientific, Singapore (1987).

[9] R. P. Feynman, Phys. Rev. Lett. **23**, 1415 (1969).

[10] O. Nachtmann, Nucl. Phys. **B38**, 397 (1972).

[11] A. Bodek *et al.*, Phys. Rev. Lett. **30**, 1087 (1973); E. M. Riordan *et al.*, Phys. Rev. Lett. **33**, 561 (1974); J. S. Poucher *et al.*, Phys. Rev. Lett. **32**, 118 (1974).

[12] A. Bodek *et al.*, Phys. Rev. **D20**, 1471 (1979).

[13] S. Stein *et al.*, Phys. Rev. **D12**, 1884 (1975).

[14] J. J. Aubert *et al.*, Phys. Lett. **B123**, 275 (1983).

[15] A. Bodek *et al.*, Phys. Rev. Lett. **50**, 1431 (1983); Phys. Rev. Lett. **51**, 534 (1983).

[16] J. Gomez *et al.*, Phys. Rev. **D49**, 4348 (1994).

[17] J. Kuti and V. F. Weisskopf, Phys. Rev. **D4**, 3418 (1971).

[18] F. E. Close, Phys. Lett. **B43**, 422 (1973).

[19] R. Carlitz, Phys. Lett. **B58**, 345 (1975).

[20] F. E. Close and A. W. Thomas, Phys. Lett. **B212**, 227 (1988).

[21] E. Eichten, I. Hinchliffe, K. Lane and C. Quigg, Rev. Mod. Phys. **56**, 579 (1984).

[22] M. Diemoz *et al.*, Z. Phys. **C39**, 21 (1988).

[23] A. D. Martin, R. Roberts and W. J. Stirling, Phys. Rev. **D50**, 6734 (1994).

[24] H. L. Lai *et al.*, Phys. Rev. **D51**, 4763 (1995); H. L. Lai *et al.*, Eur. Phys. J. **C12**, 375 (2000).

[25] N. Isgur, G. Karl and R. Koniuk, Phys. Rev. Lett. **41**, 1269 (1978); N. Isgur, G. Karl and D. W. L. Sprung, Phys. Rev. **D23**, 163 (1981).

[26] N. Isgur, Phys. Rev. **D59**, 034013 (1999).

[27] G. R. Farrar and D. R. Jackson, Phys. Rev. Lett. **35**, 1416 (1975).

[28] S. J. Brodsky, M. Burkardt and I. Schmidt, Nucl. Phys. **B441**, 197 (1995).

[29] D. F. Geesaman, K. Saito and A. W. Thomas, Annu. Rev. Nucl. Part. Sci. **45**, 337 (1995).

[30] P. R. Norton, Rept. Prog. Phys. **66**, 1253 (2003).

[31] A. W. Thomas, hep-ex/0007029 (2000). In Proceedings of HiX2000 Conference, Philadelphia, Pennsylvania, April 2000.

[32] G. B. West, Phys. Lett. **B37**, 509 (1971); W. B. Atwood and G. B. West, Phys. Rev. **D7**, 773 (1973).

[33] S. Liuti and F. Gross, Phys. Lett. **B356**, 157 (1995).

[34] W. Melnitchouk and A. W. Thomas, Phys. Lett. **B377**, 11 (1996).

[35] U. K. Yang and A. Bodek, Phys. Rev. Lett. **82**, 2467 (1999).

[36] L. W. Whitlow *et al.*, Phys. Lett. **B282**, 475 (1992).

[37] W. W. Buck and F. Gross, Phys. Rev. **D20**, 2361 (1979); F. Gross, J. W. Van Orden and K. Holinde, Phys. Rev. **C45**, 2094 (1992); J. Adam, F. Gross, S. Jeschonnek, P. Ulmer and J. W. Van Orden, Phys. Rev. **C66**, 044003 (2002).

[38] W. Melnitchouk, A. W. Schreiber and A. W. Thomas, Phys. Lett. **B335**, 11 (1994).

[39] L. L. Frankfurt and M. I. Strikman, Phys. Rep. **160**, 235 (1988).

[40] M. Botje, Eur. Phys. J. **C14**, 285 (2000).

[41] H. L. Lai *et al.*, Phys. Rev. **D55**, 1280 (1997).

[42] I. R. Afnan, F. Bissey, J. Gomez, A. T. Katramatou, W. Melnitchouk, G. G. Petratos and A. W. Thomas, Phys. Lett. **B493**, 36 (2000).

[43] I. R. Afnan, F. Bissey, J. Gomez, A. T. Katramatou, S. Liuti, W. Melnitchouk, G. G. Petratos and A. W. Thomas, Phys. Rev. **C68**, 035201 (2003).

[44] W. Melnitchouk and A. W. Thomas, Phys. Rev. **D47**, 3783 (1993) and Phys. Lett. **B317**, 437 (1993); G. Piller and W. Weise, Phys. Rep. **330**, 1 (2000).

[45] C. Ciofi degli Atti and S. Liuti, Phys. Lett. **B225**, 215 (1989); C. Ciofi degli Atti, S. Simula, L. L. Frankfurt and M. I. Strikman, Phys. Rev. **C44**, R7 (1991); S. Simula, Few Body Syst. Suppl. **9**, 466 (1995).

[46] F. Bissey, A. W. Thomas and I. R. Afnan, Phys. Rev. **C64**, 024004 (2001).

[47] C. Ciofi degli Atti, E. Pace and G. Salmè, Phys. Rev. **C21**, 805 (1980) and Phys. Lett. **B141**, 14 (1984).

[48] J. Haidenbauer and W. Plessas, Phys. Rev. **C30**, 1822 (1984).

[49] T. Y. Saito and I. R. Afnan, Few Body Syst. **18**, 101 (1995).

[50] Y. Yamaguchi, Phys. Rev. **95**, 1628 (1954).

[51] E. Pace, G. Salmè and S. Scopetta, Nucl. Phys. **A689**, 453 (2001); E. Pace, G. Salme, S. Scopetta and A. Kievsky, Phys. Rev. **C64**, 055203 (2001).

[52] S. C. Pieper and R.B. Wiringa, Ann. Rev. Nucl. Part. Sci. **51**, 53 (2001).

[53] M. M. Sargsian, S. Simula and M. I. Strikman, Phys. Rev. **C66**, 024001 (2002).

[54] C. Ciofi degli Atti and S. Liuti, Phys. Rev. **C41**, 1100 (1990) and Phys. Rev. **C44**, 1269 (1991).

[55] J. J. Aubert *et al.*, Nucl. Phys. **B293**, 740 (1987).

[56] M. Gluck, E. Reya and A. Vogt, Eur. Phys. J. **C5**, 461 (1998).

[57] A. Donnachie and P. V. Landshoff, Z. Phys. **C61**, 139 (1994).

[58] F. Gross and S. Liuti, Phys. Rev. **C45**, 1374 (1992).

[59] W. Melnitchouk, A. W. Schreiber and A. W. Thomas, Phys. Rev. **D49**, 1183 (1994).

[60] S. A. Kulagin, W. Melnitchouk, G. Piller and W. Weise, Phys. Rev. **C52**, 932 (1995); W. Melnitchouk, G. Piller and A. W. Thomas, Phys. Lett. **B346**, 165 (1995); G. Piller, W. Melnitchouk and A. W. Thomas, Phys. Rev. **C54**, 894 (1996).

[61] L. Frankfurt and M. Strikman, Nucl. Phys. **B250**, 143 (1985);

[62] S. Dieterich *et al.*, Phys. Lett. **B500**, 47 (2001); R. Ransome, Nucl. Phys. **A699**, 360 (2002).

[63] W. Melnitchouk, K. Tsushima, A. W. Thomas, Eur. Phys. J. **A14**, 105 (2002).

[64] P. Hoodbhoy and R.L. Jaffe, Phys. Rev. **D35**, 113 (1987).

[65] M. Betz, G. Krein and T.A.J. Maris, Nucl. Phys. **A437**, 509 (1985).

[66] P.J. Mulders and A.W. Thomas, Phys. Rev. Lett. **52**, 1199 (1984); M. Sato, S. Coon, H. Pirner and J. Vary, Phys. Rev. **C33**, 1062 (1986); K.E. Lassila and U.P. Sukhatme, Phys. Lett. **B209**, 343 (1988).

[67] L. H. Tao *et al.*, Z. Phys. **C70**, 387 (1996).

[68] A. Amroun *et al.*, Nucl. Phys. **A579**, 596 (1994); F.-P. Juster *et al.* Phys. Rev. Lett. **55**, 2261 (1985).

[69] D. H. Beck *et al.*, Phys. Rev. **C30**, 1403 (1984); D. H. Beck *et al.*, Nucl. Instr. Methods in Phys. Res. **A277**, 323 (1989).

[70] G. G. Petratos *et al.*, nucl-ex/0010011 (2000), in Proceedings of HiX2000 Conference, Philadelphia, Pennsylvania, April 2000; R. D. Ransome, *A Tritium Program at 12 GeV*, presented at the Workshop on Physics of Nuclei with 12 GeV Electrons, Newport News, Virginia, November 2004.

[71] H. Collard *et al.*, Phys. Rev. **138**, B57 (1965); R. W. McAllister *et al.*, Phys. Rev. **102**, 851 (1956).

[72] S. Dasu *et al.*, Phys. Rev. **D49**, 5641 (1994).

[73] D. E. Wiser, Ph.D. Thesis, University of Wisconsin (1977).

[74] I. Niculescu *et al.*, Phys. Rev. Lett. **85** (2000) 1182, 1186.

[75] F. E. Close and N. Isgur, Phys. Lett. **B509**, 81 (2001); F. E. Close and W. Melnitchouk, Phys. Rev. **C68**, 035210 (2003).

[76] J. Arrington *el.*, nuc-ex/0307012 (2004), submitted to Phys. Rev. Lett.

[77] I. Sick, Prog. Part. Nucl. Phys. **47**, 245 (2001); and references therein.

[78] J. Carlson and R. Schiavilla, Rev. Mod. Phys. **70**, 743 (1998); and references therein.

[79] H. Fenker, C. Keppel, S. Kuhn, W. Melnitchouk *et al.*, JLab experiment E03-012 (2003).

[80] S. Simula, Phys. Lett. **B387**, 245 (1996); W. Melnitchouk, M. Sargsian and M. Strikman, Z. Phys. **A359**, 99 (1997).

[81] K. Ackerstaff *et al.*, Phys. Lett. **B475**, 386 (2000).

APPENDIX I

Helium/Tritium DIS Kinematics for the $\mathbf{F_2^n/F_2^p}$ and d/u Extraction

x	W (GeV)	Q^2 $[(\mathrm{GeV}/c)^2]$	E (GeV)	E' (GeV)	θ (deg)	π/e
0.77	1.74	7.15	6.0	1.05	64.4	72
0.73	1.80	6.74	6.0	1.15	59.2	43
0.69	2.00	6.94	6.0	.640	84.5	970
0.65	2.00	5.79	6.0	1.25	52.1	28
0.61	2.00	4.88	6.0	1.74	40.0	5
0.57	2.00	4.13	6.0	2.13	33.0	2
0.53	2.00	3.52	6.0	2.46	28.3	1
0.49	2.00	3.00	6.0	2.74	24.7	0.6
0.45	2.00	2.55	6.0	2.98	21.8	0.4
0.41	2.00	2.17	6.0	3.18	19.4	0.3
0.37	2.00	1.83	6.0	3.36	17.3	0.2
0.33	2.00	1.54	6.0	3.52	15.5	0.2
0.30	2.00	1.34	6.0	3.62	14.2	0.2
0.27	2.00	1.16	6.0	3.72	13.1	0.2
0.24	2.00	0.99	6.0	3.81	11.9	0.1

Table 1: The kinematics for the proposed ^{3}He and ^{3}H inelastic cross sections measurements for the extraction of the F_2^n/F_2^p and d/u ratios as a function of the Bjorken x. The beam energy, E, is fixed at 6.0 GeV. Here, W is the invariant mass of the final hadronic state, Q^2 is minus the four-momentum transfer squared, E' is the scattered electron energy, θ is the scattered electron angle and π/e is the expected pion to electron counting ratio.

APPENDIX II

Cross Sections and Counting Rates for the $\mathbf{F_2^n/F_2^p}$ and d/u Extraction

x	$\sigma(^3\text{He})$ (nb/sr/GeV)	$\sigma(^3\text{H})$ (nb/sr/GeV)	^{3}He Rate (Events/h)	^{3}H Rate (Events/h)	^{3}He Time (h)	^{3}H Time (h)
0.77	0.0721	0.0553	390	152	38	99
0.73	0.125	0.0957	718	280	28	71
0.69	0.0791	0.0606	320	125	78	199
0.65	0.360	0.279	2380	941	10	27
0.61	1.09	0.858	9010	3610	3	7
0.57	2.73	2.19	25600	10400	1	3
0.53	6.09	4.95	61900	25600	0.5	1
0.49	12.7	10.5	136000	57300	0.5	0.5
0.45	25.0	21.0	278000	119000	0.5	0.5
0.41	46.6	39.8	527000	229000	0.5	0.5
0.37	85.1	73.8	963000	425000	0.5	0.5
0.33	152	134	1690000	759000	0.5	0.5
0.30	232	207	2500000	1140000	0.5	0.5
0.27	351	317	3610000	1660000	0.5	0.5
0.24	535	489	5100000	2370000	0.5	0.5

Table 2: Inelastic cross sections, counting rates and beam times for the different Bjorken x kinematics of the proposed ^{3}He and ^{3}H inelastic cross sections measurements for the extraction of the F_2^n/F_2^p and d/u ratios. The counting rates assume 12 cm, 11 atm gas ^{3}He and ^{3}H targets, a beam current of 100μA and a spectrometer solid angle of 6 msr.

APPENDIX III

Helium/Tritium DIS Kinematics for the $\mathbf{R} = \sigma_{\mathbf{L}}/\sigma_{\mathbf{T}}$ Measurements

x	ϵ	W (GeV)	Q^2 $[(\mathrm{GeV}/c)^2]$	E (GeV)	E' (GeV)	θ (deg)	π/e
0.24	0.21	2.30	1.40	3.6	0.50	52.3	23
0.24	0.58	2.30	1.40	4.8	1.70	23.9	6
0.24	0.76	2.30	1.40	6.0	2.90	16.3	1
0.37	0.18	2.13	2.15	3.6	0.50	66.3	29
0.37	0.56	2.13	2.15	4.8	1.70	29.8	5
0.37	0.74	2.13	2.15	6.0	2.90	20.3	0.6
0.45	0.16	2.02	2.62	3.6	0.50	74.2	34
0.45	0.55	2.02	2.62	4.8	1.70	32.9	4
0.45	0.73	2.02	2.62	6.0	2.90	22.4	0.5
0.57	0.13	1.84	3.31	3.6	0.50	85.5	46
0.57	0.53	1.84	3.31	4.8	1.70	37.2	3
0.57	0.72	1.84	3.31	6.0	2.90	25.2	0.3

Table 3: The kinematics for the proposed measurements of the $R = \sigma_L/\sigma_T$ ratio. Here, x is the Bjorken scaling variable, ϵ is the degree of the longitudinal polarization of the virtual photon, W is the invariant mass of the final hadronic state, Q^2 is minus the four-momentum transfer squared, E and E' are the incident and scattered electron energies, θ is the scattered electron angle and π/e is the expected pion to electron counting ratio.

APPENDIX IV

Counting Rates and Beam Times for the $\mathbf{R} = \sigma_{\mathbf{L}}/\sigma_{\mathbf{T}}$ Measurements

x	ϵ	^{3}He Rate (Events/h)	^{3}H Rate (Events/h)	^{3}He Time (h)	^{3}H Time (h)
0.24	0.21	48900	22500	0.5	1.5
0.24	0.58	489000	225000	0.5	0.5
0.24	0.76	1400000	646000	0.5	0.5
0.37	0.18	14600	6380	2	5
0.37	0.56	155000	67700	0.5	0.5
0.37	0.75	471000	206000	0.5	0.5
0.45	0.16	7290	3110	4	10
0.45	0.55	78800	33700	0.5	1
0.45	0.73	245000	105000	0.5	0.5
0.57	0.13	2590	1070	12	28
0.57	0.53	28400	11700	1	3
0.57	0.72	89900	37100	0.5	1

Table 4: Counting rates and beam times for the measurements of the $R = \sigma_L/\sigma_T$ ratio. Here, x is the Bjorken scaling variable and ϵ is the degree of the longitudinal polarization of the virtual photon. The counting rates assume 12 cm, 11 atm gas ^{3}He and ^{3}H targets, a beam current of 100μA and a spectrometer solid angle of 6 msr.